Spatial modelling of gully erosion in the Ardib River Watershed using three statistical-based techniques

Alireza Arabameri[1], Biswajeet Pradhan[2,3]*, Dieu Tien Bui[4]*

[1]Department of Geomorphology, Tarbiat Modares University, Tehran 36581-17994, Iran; Email. Alireza.ameri91@yahoo.com
[2]Centre for Advanced Modelling and Geospatial Information Systems, Faculty of Engineering and Information Technology, University of Technology Sydney, New South Wales, Australia. Email. Biswajeet.Pradhan@uts.edu.au
[3]Department of Energy and Mineral Resources Engineering, Sejong University, Choongmu-gwan, 209 Neungdong-ro Gwangjin-gu, Seoul, 05006, Republic of Korea. Email biswajeet24@gmail.com
[4]Institute of Research and Development, Duy Tan University, Da Nang 550000, Vietnam

* Corresponding author: biswajeet.pradhan@uts.edu.au; Dieu.TienBui@gmail.com

Abstract

Gully erosion threatens land sustainability. Gullies trigger considerable erosion, damaging agricultural land, infrastructure and urban areas; thus, predicting and modelling gully susceptibility is of utmost concern. In particular, such a model is urgently required in semiarid areas where soil loss from gullies is high. Three predictive models are evaluated to assess gully erosion susceptibility mapping (GESM) in Semnan Province, Iran. The index of entropy (IOE), frequency ratio (FR) and certainty factor (CF) models are combined with remote sensing and geographic information system techniques to predict gully erosion. The collation of data from geographic resources identified 287 gullies in the study area. These areas were then randomly divided into 2 groups for calibration (70% or 201 gullies) and validation (30% or 86 gullies). Pairwise linear dependency amongst geoenvironmental factors was also assessed. A total of 16 factors were screened for modelling. Four performance metrics, namely, true skill statistic (TSS), area under the receiver operating characteristic (AUROC) curve, seed cell area index (SCAI) and modified SCAI (mSCAI), were used to evaluate the prediction accuracy and robustness of each model using validation datasets. Bootstrapped replicates were considered in estimating the accuracy and robustness of each model by varying gully/no-gully samples. The IOE results indicated that elevation, lithology and slope angle promoted favourable conditions for gully erosion in the study area. The results showed that the IOE model performed better than the FR and CF models for all three validation datasets ($AUROC_{mean}$ = 0.874 and TSS_{mean} = 0.855). This finding was also confirmed in terms of stability and robustness (R_{TSS} = 0.024 and R_{AUROC} = 0.023). The SCAI and mSCAI results showed that all the models exhibited acceptable accuracy, but IOE demonstrated superior performance. Accordingly, IOE was used as the reference model for the study area, indicating that 19.75% and 9.44% of the study area are included in the predicted high and very high susceptibility classes, respectively. Considering the accuracy of GESM, IOE is a reliable tool for decision-making, management and land use planning within the region.

Keywords: Gully erosion susceptibility; Statistical model; Index of entropy; GIS; Semnan Province; Iran

1. Introduction

A review of scientific papers shows that approximately 58% of land degradation worldwide is due to soil erosion (Arekhi and Niazi, 2010). Most of land degradation events began after World War II, reducing production by 17% and causing extensive environmental damage. Therefore, erosion prevention is considered one of the most important issues in natural resource conservation (Hengl, 2006). Gully erosion, which is a destructive form of soil erosion in arid and semiarid regions (Arabameri et al., 2018d), threatens land sustainability. This phenomenon is due to the high erosion rates triggered by gullies, and it results in damage to agricultural land, infrastructure and urban areas. Gully susceptibility should be urgently predicted and modelled, particularly in semiarid areas where soil loss is high and extreme when gullies develop. The awareness of gully erosion risk in a watershed will enable the identification of critical areas and the prioritisation of management and conservation programmes. Awareness is achieved by adopting complex numerical models to calculate the two-phase, water- and soil-transport balance. These models include OpenLISEM (Bout et al., 2018) and SIMWE (Fernandez et al., 2017). The limited availability of spatially distributed physical parameters (i.e. input data) hinders the feasibility and reliability of deterministic models due to inherited uncertainties. The lack of consistency in space and time of soil erosion measurements increases the difficulty of achieving a meaningful assessment and validation of results.

The alternatives to deterministic approaches, at least in the early stages of most research, are spatial-based predictive models. These models are used to estimate the potential proneness of areal units to gullying on the basis of the analysis of existing gullies. These models also provide insights into the preparation of quantitative soil erosion maps (Dabral et al., 2008).

Given the spatial extent of most basins in Iran, implementing erosion prevention measures over the entire watershed is difficult and economically infeasible. To tailor preventive and protective actions, locations that will most likely experience gully formation should be identified and prioritised. Appropriate and effective management plans can only be implemented after identifying locations with high erosion potential (Naderi et al., 2008).

Several methods have been developed for gully erosion susceptibility mapping (GESM) using spatial predictive models. In contrast with deterministic models, the major advantage of these approaches is that they produce relevant information for decision makers and require less complex data (Wang et al., 2003). Most of the required data can be compiled by combining remote sensing (RS) data and geographic information system (GIS) software. Data management and computation in GIS can generate gully erosion maps with low costs and acceptable accuracy even for extensive areas (Shi et al., 2004). GIS enables rapid and intuitive representation and analysis of spatial data and can generally incorporate information layers from diverse sources (Sharma and Mahajan, 2018).

Given its functional agility, GIS has been successfully adopted in numerous environmental risk assessments. The development and inclusion of internal, reproducible routines via ‘model builder’ techniques can visually transform scripts, such as Python codes, and codes can be stored and run. Consequently, input and output can be controlled consistently, along with data processing, modelling and validation tasks within a single work pipeline (Sharma and Mahajan, 2018).

In addition, increasing computational capacity has resulted in the development of a wide array of models for identifying areas susceptible to gully erosion. These models can be classified into three groups: (i) joint multi-criteria decision-making and analytic hierarchy process (AHP) models (Arabameri et al., 2018c); (ii) bivariate and multivariate statistical models, including frequency ratio (FR) (Rahmati et al., 2016; Meliho et al., 2018), information value (Conforti et al., 2011; Arabameri et al., 2019b), conditional probability (Mojaddadi et al., 2017), evidential belief function (Arabameri et al., 2018a), certainty factor (CF) (Azareh et al., 2019), index of entropy (IOE) (Aghdam et al., 2016; Youssef et al., 2015), logistic regression (Kornejady et al., 2015; Arabameri et al., 2018a) and weight of evidence (Dube et al., 2014); and (iii) machine learning models, such as maximum entropy (Zakerinejad and Maerker, 2014; Kornejady et al., 2017), multivariate adaptive regression spline (Gomez-Gutierrez et al., 2015), artificial neural network (Pradhan and Lee, 2010; Zare et al., 2013), adaptive neuro-fuzzy inference system (Dehnavi et al., 2015; Mojaddadi et al., 2017), boosted regression tree (Amiri et al., 2019), random forest (RF) (Arabameri et al., 2018b), linear discriminant analysis (LDA) (Arabameri and Pourghasemi, 2019), support vector machine (SVM) (Pourghasemi et al., 2017), bagging best-first decision tree (Hosseinalizadeh et al., 2019) and classification and regression trees (Arabameri et al., 2018b).

In Iran, gully erosion is a serious environmental issue that threatens local economies (Arabameri et al., 2019a). In the arid and semiarid Isfahan Watershed, gully erosion has been reported to damage agricultural lands, roads, power transmission grids, railway lines, irrigation and water supply channels, extraction facilities and mineral and oil and gas refineries. Gullying affects arterial road networks within cities, industrial facilities, forests, pastures, dams, natural and artificial lakes, farms and residential areas, and thus, its prevention and mitigation are extremely important to local communities. Accordingly, the current study aims to assess the potential proximal causes of gully erosion and susceptibility to gully erosion to provide information to local agencies that develop comprehensive management plans. Considering the numerous models available in the literature, comparative studies are becoming increasingly popular to identify the standard or best model on the basis of predictive performance. Improved predictive models (gully erosion susceptibility models in this case) can significantly reduce costs and help direct effort towards the most susceptible locations. To accomplish this objective, the effectiveness of three statistical models, namely, IOE, CF and FR, is assessed to develop a GESM for the Ardib Watershed.

The major disadvantage of data mining methods is their inability to calculate the spatial relationship between conditioning factors and gully locations. Bivariate statistical models, such as IOE, can address this issue and calculate the relative weights of conditioning factors on the occurrence of gully erosion.

2. Material and Methods

2.1 Study area

The Ardib Watershed (area = 4209 km^2) lies at 54° 55′ 08″ N and 55° 42′ 31″ N and 32° 52′ 13″ E and 33° 38′ 23″ E (Fig. 1). The area is mostly flat, with elevations ranging from 644 metres above sea level (m.a.s.l.) to 2291 m.a.s.l., with an average of 935 m. The maximum slope is 72.70°, with an average of 4.35°. The climate is arid, and the average annual rainfall and temperature are 85.30 mm and 18.93 °C, respectively (IRIMO, 2012). Limestone, sandstone, marl, shale and red conglomerate are the most common lithotypes (GSI, 1997). Low- (36.54%) and moderate-quality pasture (13.37%) and bare lands (9.34%) are the land uses that cover the largest areas of the region. Soil is primarily entisols and aridisols (Soil Survey Staff, 2014). These environmental characteristics render the area extremely susceptible to gully erosion. Erodible soil is frequently ignored and even abandoned. Infrequent rainfall events enhance the problem of gully erosion susceptibility, but heavy rainfall becomes the norm once precipitation occurs. For example, a single precipitation event in these areas can occasionally account for 60% of the annual rainfall in only less than a few hours. The study area is situated in the Sanandaj–Sirjan geological structural zone of Iran (Alavi, 1994). The structural geology of this area is similar to that of Zagros, and this area is also called the Inner Zagros (Stocklin, 1968). The rock units are composed of sediment sequences related to the Mesozoic strata in the Ardib Basin. These units have undergone metamorphism in the low greenschist facies. The effects of metamorphism are weak in terms of schistosity on shaley and marly units and in terms of recrystallisation on carbonate units. A series of major and minor faults has been observed in the rock units of the region. The most important faults are thrust faults, which occur in the northern and eastern basins. These faults have been formed by the drift of Middle Cretaceous rock units. The direction of these faults is northwest–southeast, and the fault plane is towards the northeast. Regional geomorphology and geology strongly control the development of gully occurrences in the study area. Geomorphologically, the study area consists of 44% piedmont landscape, including fluvial, alluvial fans and continuous fans (Bahada), old bahada and piedmont plains; 22% mountain landscape, including discontinuous alpine landforms; and 34% alluvium plain landscape, including alluvial and river terraces.

2.2 Methodology

This study involved three major steps (Fig. 2): (i) database preparation, (ii) GESM calculation and mapping and (iii) result validation. The first step comprised several nested subphases. A gully erosion inventory was conducted. The locations of gully erosion were divided into training and validation sets. The values of gully erosion conditioning factors were determined using satellite imagery, preexisting thematic maps and a digital elevation model (DEM).

Several steps were used to pre-process the DEM using ArcHydro: (i) identification and filling of the sinks of the Advanced Land Observing Satellite DEM (ALOS DEM). If the DEM contains flat area, mostly produced by the method of filling sinks, one can not use the simple aspect based on the flow model, therefore, in this research we used from (Planchon and Darboux, 2002) method of filling sinks which produced no flat areas to handle the flat area problem, (ii) calculation of the flow direction using the filled DEM, iii) determination of the flow accumulation using the D8 algorithm (O'Callaghan and Mark, 1984). This algorithm is simple and traditional, therefore it is the most commonly used cell-based runoff model. To generate the stream network from the D8 model, we must define a threshold value serving as a minimum value when selecting cells with catchment areas for streams, (iv) estimation of the appropriate threshold to extract the stream network, (v) determination of the threshold (500 cells) for extracting the stream network, (vi) calculation of the stream order using flow direction, (vii) conversion of grid stream files to vector features and (viii) delineation of the drainage basin using flow direction. FR, IOE and CF were tested as probabilistic models. The area under the receiver operating characteristic (AUROC) curve, true skill statistic (TSS), seed cell area index (SCAI) and modified SCAI (mSCAI) metrics were used to assess model performance using validation datasets.

2.3 Data preparation

GESM necessitates building a map that shows the spatial distribution of the gullies (Arabameri et al., 2019a). Our gully erosion inventory map was digitised from the archive of the Isfahan Agricultural and Natural Resources, Research and Education Centre (http://esfahan.areeo.ac.ir/). To complete and validate this inventory, Google Earth images were visually interpreted and extensive field surveys were conducted in the study area. A total of 287 gully head cuts were identified (Fig. 1), and these areas were randomly divided into two groups to support calibration (70% or 201 gullies) and validation (30% or 86 gullies) (Arabameri et al., 2019b). Using the two occurrence subsets for reference, an equal number of absence cases (i.e. locations without gully erosion) was merged with the respective subset. In spatial modelling, approximately equal proportions of gully-present (1) and gully-absent (0) pixels (Conoscenti et al., 2014; Pourghasemi et al., 2017; Arabameri et al., 2019b) should be generally obtained. Hence, 287 gully-present pixels were randomly selected to be used along with the 287 gully-absent pixels (Conoscenti et al., 2014; Angileri et al., 2016).

This step ensures that the final probability distribution will be bounded between 0 and 1, simplifying the interpretation of the susceptibility map (Camilo et al., 2017) because the upper probability boundary will not achieve extremely small values, such as that in unbalanced datasets (Lombardo and Mai, 2018). This operation was repeated six times to account for the variability in data (Fig. 3). A single replicate may perform satisfactorily because of the randomisation procedure. However, several replicates can reconfirm the predictive power of a model. Theoretically, the larger the bootstrap sample, the higher the confidence in the robustness (limited variance amongst replicates) of the model. The specific computational requirements of models may prohibit many replicates, and few replicates are computed when the computational burden is heavy (Lombardo et al., 2018b). Hundreds or even thousands of bootstrapped replicates can be frequently created (Lombardo et al., 2018a), particularly when models are run quickly. The area under receiver operating characteristic (AUROC) and TSS values of each replicate were calculated. Then, the mean of each replicate was considered for validation. Several identified gullies in the study area are shown in Fig. 4.

From the characteristics of the study area, the scale of the analyses and the multi-collinearity test results, 16 gully erosion conditioning factors (GECFs) were included to assess their relationships to the spatial distribution of gullies, namely, elevation (Fig. 5a), slope (Fig. 5b), aspect (Fig. 5c), plan curvature (Fig. 5d), topographic wetness index (TWI - Fig. 5e), stream power index (SPI - Fig. 5f), convergence index (CI - Fig. 5j), slope length (LS - Fig. 5h), drainage density (Fig. 5i), distance to stream (Fig. 5g), distance to road (Fig. 5k), distance to fault (Fig. 5i), normalised difference vegetation index (NDVI - Fig. 5m), land use and land cover (LULC - Fig. 5n), soil type (Fig. 5o) and lithology (Fig. 5p).

The ALOS DEM with a resolution of 12.5 m downloaded from the Alaska Satellite Facility Distributed Active Archive Centre was used to extract the topographical and hydrological data of map elevation, slope, slope aspect, plan curvature, LS, TWI, SPI, CI, distance to stream and drainage density (Arabameri et al., 2019b, 2019c). The reproduction of the complex morphology and features depends on accuracy and gridding techniques (Boreggio et al., 2018; Wu et al., 2019). The quality of reproduction influences the value of several topographical and hydrological GECFs. Therefore, an ALOS DEM with a vertical accuracy of 0.3 m was used in this research. Similar to the accuracy assessment procedures implemented by Gesch et al. (2012), the vertical accuracies of the ALOS DEM were assessed by comparing ALOS DEM elevations with those of the ground control points (GCPs). At each point, DEM elevations were extracted using ArcGIS 10.5 software. Then, the differences in elevation were computed by subtracting the GCP elevation from its corresponding DEM elevation. These differences are the measured errors in the ALOS DEM. For a particular DEM, positive errors represent locations where the DEM was above the GCP elevation, and negative errors occur at locations where the DEM was below the control point elevation. From these measured errors, the mean error and the root-mean-square error for each DEM were calculated, including the standard deviations of the mean errors. The mean error (or bias) indicates if a DEM has an overall vertical offset (either positive or negative) from the true ground level (Gesch et al., 2012). Lastly, the accuracy assessment results were analysed. The details regarding how the ALOS DEM was produced using interferometric synthetic aperture radar (InSAR) were discussed by Zhou et al. (2005) and Zhang et al. (2012). The most important step in InSAR for DEM generation is phase measurement, followed by the transformation of phase to height (Zhou et al., 2005).

The simple difference method (Jones, 1998) was applied to extract the slope angles of the study area using equations 1-3:

$$Slope\ angle = arctan\sqrt{f_x^2 + f_y^2} \qquad (1)$$

$$f_x = \frac{z_8 - z_2}{2w} \qquad (2)$$

$$f_y = \frac{z_6 - z_4}{2w} \qquad (3)$$

where $z_1$to z_9 are cells of the 3 × 3 moving window and W is the grid resolution, which is equal to 12.5 meters in this study.

Slope aspect is defined as the direction of the slope (Zhou and Liu, 2004). In this study, the slope aspects of the study area were extracted from the DEM by applying equation 4 (Zhou and Liu, 2004):

$$aspect = 270^{\circ} + arctan\left(\frac{f_y}{f_x}\right) - 90^{\circ}\frac{f_x}{|f_y|}^{\circ} \qquad (4)$$

Plan curvature is defined as curvature in a horizontal plane. In addition, a plan curvature can be defined as the hypothetical line, which crosses a specific cell on the contour line. Plan curvature is derived using the following equation (Evans, 1979):

$$plan\ curvature = \frac{((z_4+z_9)/2 - z_5)}{2w} \quad (5)$$

Convergence index is a terrain parameter, which show the structure of the relief as a set of convergent areas (channels) and divergent areas (ridges). It represents the agreement of the aspect direction of surrounding cells with the theoretical matrix direction. The values range from -100 (max divergent, real peaks and ridges) by 0 (planar areas) to 100 (max convergent, real pits and channels). If there is maximum agreement with divergent matrix the convergence index is (0 - 90) × 10/9 = -100. If there is ideal sink (maximum convergence) the convergence index is (180 -90) × 10/9 = 100.

TWI, SPI and LS can be obtained using the following equations (Moore and Burch, 1986; Moore et al., 1991):

$$\mathrm{TWI} = \mathrm{In}\ (A_S/\tan\beta), \quad (6)$$

$$SPI = As\ \times \tan\sigma, \quad (7)$$

$$LS = \left({}^{fa \times cellsize}/_{22.13}\right)^{0.4} \times \left({}^{sin\sigma}/_{0.0896}\right)^{1.3}, \quad (8)$$

where A_S is the specific catchment area of the basin (m^2/m), β is the slope steepness (°), fa is the flow accumulation and σ is the slope (°).

A Landsat 8 operational land imager and thermal infrared sensor (OLI/TIRS) scene collected on July 21, 2018 (Path 162/Row 34) with a spatial resolution of 30 m and 15 m for the visual and panchromatic bands, respectively (https://earthexplorer.usgs.gov/), was used to compute NDVI through Eq. 9:

$$NDVI = {}^{IR - R}/_{IR + R}, \quad (9)$$

where IR and R denote the infrared and red portions, respectively, of the electromagnetic spectrum.

A 1:50,000-scale topographic map obtained from the National Geographic Organisation of Iran (www.ngo-org.ir) was used to digitise the road network. Stream networks in the study area were extracted from ALOS DEM with a spatial resolution of 12.5 m. A detailed explanation of the calculation of the drainage network from DEM can be found in Youssef and Pradhan (2010) and Lin and Oguchi (2004). General DEM sinks were identified and filled for determination of flow direction and flow accumulation. The critical threshold is the minimum upstream drainage required to initiate a stream. By analysing three different threshold values, we can see that if the values we choose is too small, errors can be detected even along streams that are correctly determined. These errors can be eliminated by increasing the threshold values, but after this modification, the number of determined streams will be decreased. There is no general rule to establish threshold values (Kiss, 2004). Among other things the optimal scale of threshold may depend on the scale of the model or the morphological and geological characteristics (e.g. drainage density, relief energy etc.) of the area. In the present study, a threshold of greater than 500 was used to generate drainage.The Landsat 7 Enhanced Thematic Mapper Plus (ETM+) image with a spatial resolution of 30 m (Path/Row: 162/34; observation day: May 25, 2002; https://earthexplorer.usgs.gov/), was used in ENVI4.7 software to produce the fault map of the Ardib Watershed (Ali and Pirasteh, 2004). Photogeological techniques for structural studies have been implemented in different parts of the world (Ramasamy, 1985; Iqbaluddin and Ali, 1986; Ramsay and Hubber, 1987; Rangzan, 1993).

ALOS DEM was imported to ENVI 4.7 and overlaid on the ETM+ image to create 3D surface views, increasing the enhancement of structural features, such as faults, for easy recognition and interpretation. Major and minor faults and fractures were accurately identified using the image visualisation process. To illustrate the images, a series of spatial filters was used. The filters used in this study were high-pass and sun angle filters. The Euclidean distance and line density tools in ArcGIS 10.5 were used to prepare distances to roads, streams and fault and drainage density.

The lithology layer was developed by digitising the geological map (Bayazeh sheet at 1:100,000 scale) obtained from the Geological Society of Iran (GSI; http://www.gsi.ir/; 1997). The lithology map was prepared from an available 1:100,000-scale geological map. The Ardib Watershed contains various geological formations (Table 1). The spatial distribution of the lithology units in the study area is shown in Fig. 5p.

A soil type map (1:100,000) was obtained from the Isfahan Agricultural and Natural Resources Research Centre and classified into six categories. The LULC map of the study area was generated using Landsat 8 OLI/TIRS images (Path 162/Row 34). To create the LULC map, supervised classification using the maximum likelihood algorithm was applied. A total of 456 GCPs were selected for validation using the kappa index. The obtained kappa coefficient for the prepared map was 0.907, indicating its high accuracy.

All the data layers for the GECFs used for GESM were converted into raster coverage and reprojected onto a common projection with a resolution of 12.5 m × 12.5 m to correspond to the DEM. The GECFs and their sources, scales and classes for gully erosion modelling are presented in Table 2.

2.4 Models

2.4.1 IOE

Entropy modelling, which was first presented by Shannon (1948), is one of the approaches that can address irregularities and uncertainties in a given numerical system (Yufeng and Fengxiant, 2009). The following equations were used to determine the location and likelihood of gully erosion and to calculate the relative importance of each effective factor for predicting gully erosion (Youssef et al., 2015):

$$\left(\mathrm{P_{ij}}\right) = \frac{\mathrm{FR}}{\sum_{\mathrm{j=1}}^{\mathrm{Sj}} \mathrm{FR}}; \qquad (10)$$

$$\mathrm{H_j} = -\sum_{\mathrm{i=1}}^{\mathrm{Sj}} \left(\mathrm{P_{ij}}\right) \log_2 \left(\mathrm{P_{ij}}\right),\ \mathrm{j} = 1, \dots, \mathrm{n}; \qquad (11)$$

$$\mathrm{H_{\,max}} = \log_2 \mathrm{S_j} \quad \mathrm{S_j} - \text{number of classes}; \qquad (12)$$

$$\mathrm{I_j} = \frac{\mathrm{H_{\,j\,max}} - \mathrm{H_J}}{\mathrm{H_{\,j\,max}}}, \mathrm{I} = (0,1),\ \mathrm{j} = 1, \dots, \mathrm{n}; \qquad (13)$$

$$\mathrm{W_J} = \mathrm{I_j}\ \mathrm{P_{ij}}; \qquad (14)$$

where (P_{ij}) is the probability density; H_j and H_{jmax} represent the entropy and maximum entropy values, respectively; I_j is the information value; S_j is the number of categories and W_j represents the resultant weight value for each factor. The range of W_j is between 0 and 1. After computing the final weight of each factor and their classes, these values were applied to their respective raster layer. Lastly, the values were summed to produce a final GESM using Eq. 15, which is a direct operation in ArcGIS that is solved using the weighted sum tool (Haghizadeh et al., 2017).

$$GESM = \sum_{I=1}^{n} \left(W_J \times P_j\right), \qquad (15)$$

where W_j and P_j are the final weight and probability density, respectively, of the *jth* feature.

2.4.2 FR

The FR model is a simple probabilistic model that calculates the relationship between a dependent (gully erosion probability) and independent variables (conditioning factors) (Oh et al., 2011; Wang and Li, 2017). The FR model is defined by Rahmati et al. (2016) as follows:

$$FR = \frac{A/B}{C/D}, \qquad (16)$$

where A is the number of pixels with gully erosion for each factor, B is the total gully inventory in the study area, C is the number of pixels in each class of factors and D is the number of total pixels in the study area. The results of each factor are combined in a GIS environment to obtain the gully erosion sensitivity index.

$$GEI = \sum (FR)_i \qquad (i = 1,2,3, \dots, n); \qquad (17)$$

where GEI is the gully erosion index and I is the number of factors. If the FR weight is greater than 1, then a positive correlation exists between the dependent and independent variables. Values less than 1 indicate a weak correlation relationship (Razavizadeh et al., 2017).

2.4.3 CF

CF can solve the layer integration problem (Heckerman, 1986; Lan et al., 2004). In this model, the thematic layers of the conditioning factors are integrated into the gully inventory map in GIS. The CF values for each layer are calculated to produce a susceptibility map. The layers are integrated in accordance with the standard integration equation to determine the final CF and sensitivity classes (Arabameri et al., 2019a). The CF model is calculated as follows:

$$CF = \begin{cases} \frac{P_a - P_b}{P_a(1-P_b)} & if\ P_a \geq P_b \\ \frac{P_a - P_b}{P_b(1-P_a)} & if\ P_a < P_b \end{cases}, \qquad (18)$$

where P_a is the conditional probability of the gully erosion occurring within class a and P_b is the prior probability related to the occurrence of gully erosion in all the independent variable classes. Thereafter, each independent variable is analysed in pairs using Eq. 18. During this stage, three modes emerged based on the positive and negative values of the pixel value in the two raster layers.

$$Z = \begin{cases} X + Y - XY, & X, Y \geq 0 \\ \frac{X+Y}{1-\min(|X|,|Y|)}, & X \times Y < 0; \\ X + Y + XY, & X, Y < 0 \end{cases} \qquad (19)$$

where X and Y are the two investigated independent variables. Lastly, the raster layer of the Z index is obtained using the intersection and computation of all their pixels. By using the raster calculator and the CON conditional function, analysis can be conducted on any of the variables in pairs. Then, the layer obtained from the Z index is analysed using the third raster layer. The conditional calculations for the pixels of all the raster layers of the independent variables are performed.

2.5. Multicollinearity analysis (MCA)

Before using the geoenvironmental factors and their combinations in gully erosion susceptibility map preparation based on the models, the conditional independence amongst the data used should be examined. If the data are conditionally independent, then these data can be used in the models. MCA indicates the amount of correlation amongst the GECFs (independent variables) (Arabameri et al., 2018a). Tolerance (TOL) and the variance inflation factor (VIF) are popular and efficient indices for MCA (Cama et al. 2017) that do not have standardised thresholds. However, the intervals of ≤5 or 10 for VIF and ≤0.1 or 0.2 for TOL are widely used by researchers to imply that no collinearity is present and that gully conditioning factors are independent (O’brien, 2007).

2.6 Analysis of data accuracy and robustness

The data used for modelling are not used for validation; thus, the gully dataset is divided into two groups for calibration (70%) and validation (30%) purposes (Arabameri et al., 2019a). The AUROC, TSS, SCAI and mSCAI models are used for validation. Eqs. 20 to 23 are used to calculate AUROC and TSS (Fukuda et al., 2013).

$$AUROC = \begin{cases} \mathrm{x} = 1 - \mathrm{specificity} = 1 - \left[\frac{\mathrm{TP}}{(\mathrm{TN}+\mathrm{FP})}\right] \\ \mathrm{y} = \mathrm{sensitivity} = \left[\frac{\mathrm{TP}}{(\mathrm{TP}+\mathrm{FN})}\right] \end{cases}, \quad (20)$$

$$TSS = TPR - FPR, \quad (21)$$

$$TPR = \frac{TP}{TP+FN}, \quad (22)$$

$$FPR = \frac{FP}{FP+TN}, \quad (23)$$

where true positive (TP) and true negative (TN) are the number of pixels that are correctly classified and false positive (FP) and false negative (FN) are the numbers of pixels that are erroneously classified. The TP rate (TPR) indicates the proportion of gully pixels that are correctly classified as gully occurrences. The FP rate (FPR) reflects the proportion of non-gully pixels that are incorrectly classified as gully.

The AUROC value is between 0.5 and 1; a high value indicates a strong model, whereas a low value signifies a weak model (Hong et al., 2017). The AUROC values can be classified into four classes of accuracy: poor (AUROC = 0.6 to 0.7), fair (AUROC = 0.7 to 0.8), good (AUROC = 0.8 to 0.9) and excellent (AUROC= 0.9 to 1) (Fressard et al., 2014). For TSS, a high value signifies a strong model (Fukuda et al., 2013).

SCAI was used to evaluate the classification accuracy of the models. This index represents the ratio computed between the percentage of the area in each gully susceptibility class and the percentage of the gullies occurring in that class (Yilmaz, 2009). High SCAI values in the very low susceptibility class and low values in the very high susceptibility class indicate accurate classification. To obtain a satisfactory model comparison, the areas of the susceptibility classes were weighted with respect to the corresponding densities of gullies in the validation set using mSCAI.

$$mSCAI = \frac{A}{B}, \qquad (24)$$

where A is the aerial extent of the susceptibility classes (%) and B is the gully of the validation set in each susceptibility class (%). mSCAI was introduced by Suzen and Doyuran (2004). In accordance with mSCAI, the best model should detect gullying without classifying large areas of the map as unstable to reflect the typically low density of the event. Moreover, the model should possess the highest percentage of gullies in areas classified as highly and very highly susceptible.

To compare the susceptibility models based on the location of major differences, two of the obtained maps were overlaid. When the two maps classified a pixel under the same susceptibility class, spatial agreement was considered ‘correct’. When the classification of a pixel in the two maps differed by only one susceptibility class, the agreement was considered ‘acceptable’; a larger difference was tagged as ‘unacceptable’ or ‘mismatch’ (Lucà et al., 2011).

Model robustness can be calculated and checked by analysing the changes in model accuracy when input data are changed (Cama et al., 2017; Pourghasemi et al., 2017; Rahmati et al., 2019). The robustness of a model is determined by randomly changing the validation datasets and differentiating the maximum and minimum accuracy values on the basis of each evaluation criterion (Conoscenti et al., 2014).

$$R_{TSS} = TSS_{max} - TSS_{min}, \qquad (25)$$

$$R_{AUC-ROC} = AUC - ROC_{max} - AUC - ROC_{min}, \qquad (26)$$

where R_{TSS} and R_{AUROC} are the robustness measures of a model based on the TSS and AUROC criteria, respectively. TSS_{max} and $AUROC_{max}$ are the maximum accuracy values, and TSS_{min} and $AUOC_{min}$ are the minimum accuracy values.

3. Results

3.1 Independence analysis of the conditioning factors

The results of the multicollinearity test (Table 3) show that amongst the 19 conditioning factors initially selected in this study, 3 factors, namely, rainfall (TOL = 0.032 and VIF = 31.63), catchment area (TOL = 0.028 and VIF = 35.65) and soil texture (TOL = 0.022 and VIF = 45.23), were collinear. Consequently, these factors were excluded in the modelling phase, leaving 16 conditioning factors to predict gully erosion susceptibility.

3.2 GESM

The spatial associations between each conditioning factor and the gullies identified in the inventory are summarised in Table 4 for FR and CF and those for IOE are displayed in Fig. 6. Elevation (class 802–954 m, CF = 1.93 and FR = 2.93), slope (class 5°–10°, CF = 0.68 and FR = 2.28), aspect (southeast facing class, CF = 0.84 and FR = 1.84) and planar curvature (concave class, CF = 0.04 and FR = 1.04) are strongly correlated and positively contribute to gully formation. Similarly, TWI, SPI, CI and LS, with respective classes of >11.7, 13.1–15.8, −12.1–11.3 and >22.9 m, contributed to gully susceptibility (CF: 0.30, 0.51, 0.39 and 0.61 and FR: 1.43, 2.05, 1.49 and 2.58, respectively).

Our methods considered potential nonlinearities between gullies and conditioning factors. A linear model would have produced a single weight for the entire factor distribution, but reclassifying into several classes increases flexibility. Therefore, only the classes that are strongly associated with erosion susceptibility were reported, i.e. whether these classes belong to one or multiple cases.

Strong pairwise influences were found between gullying and drainage density (0.89–1.34 km/km^2), distance to stream (<100 m), distance to the road (1000–1500 m) and distance to fault (<500 m). The four classes indicated that factor influence on the final model is minimal (<0.89 km/km^2, CF = −0.49 and FR = 0.51; 300–400 m, CF = −0.48 and FR = 0.68; >2500 m, CF = −0.83 and FR = 0.55; 1500–2000 m, CF = −0.85 and FR = 0.15, respectively).

For NDVI, LULC, soil type and lithology, only the following classes were significant: 0.044–0.12, poor pasture, aridisols and C group geology units (including limestone, sandstone, marl, shale and red conglomerate), with associated CF (0.50, 1.05, 0.38 and 1, respectively) and FR (1.50, 2.05, 1.38 and 3.53, respectively).

The factors that exert the greatest impact on gully formation based on the IOE modelling process were elevation (1.61), lithology (0.441) and slope angle (0.424). These factors were followed by distance to road (0.358), NDVI (0.318), drainage density (0.209), LULC (0.196), soil type (0.177), distance to fault (0.155), LS (0.066), slope aspect (0.060), SPI (0.033), convergence index (0.028), distance to stream (0.017) and plan curvature (0.011).

The values of the resulting GESMs obtained using the three methods differed: IOE (0.960–6.55), FR (8.55–29.45) and CF (−0.654–0.871). To make these results comparable, each raster map was binned into five classes using the natural break method, i.e. from very low to very high susceptibility (Fig. 7). Each model distinctly depicted spatial proneness to gully erosion (Table 5). FR classified 24.29% of the area under very low susceptibility, 44.65% under low susceptibility, 14.35% under moderate susceptibility, 14.46% under high susceptibility and 2.25% under very high susceptibility. The CF model assigned 21.8%, 35%, 22.81%, 15.29% and 5.11%, for the respective categories, and IOE predicted 15.42%, 26.46%, 28.92%, 19.75% and 9.44%, respectively.

3.3 Evaluation of the GESM

The estimated bootstrapped predictive metrics for each replicate in validation datasets are presented in Table 6 and Fig. 8. From the AUROC values, IOE ranged from 0.865 to 0.894 (mean = 0.874), FR ranged from 0.859 to 0.883 (mean = 0.868) and CF ranged from 0.853 to 0.879 (mean = 0.865). The TSS values of the IOE, FR and CF models ranged from 0.855 to 0.830, 0.811 to 0.879 and 0.870 to 0.861, respectively, with respective means of 0.864, 0.851 and 0.84. The AUROC and TSS metrics suggest that all the models exhibit satisfactory performance. IOE achieved the highest accuracy amongst the three. Moreover, the results of SCAI (Table 7) consistently indicated a reasonable classification accuracy.

The obtained mSCAI values (Fig. 9) indicate that the susceptibility map developed using the IOE model is more accurate than the other bivariate models. This model correctly located approximately 88.37% of the gullies in the zones with very high and high susceptibility even though the cumulative areal extent is only approximately 29.1% of the map.

The comparison of the models based on spatial agreement show that the CF–RF model (Fig. 10), with 48% correct, 37% acceptable and 15% unacceptable results, demonstrated the least variation amongst the models. By contrast, the CF–IOE model, with 21% correct, 32% acceptable and 47% unacceptable results exhibited the largest variation in the entire area.

Robustness was estimated on the basis of AUROC and TSS (Fig. 11). All the models maintained stability during the validation step, and only slight variations were observed. The IOE model consistently produced analogous predictive results despite random changes in the dataset. Furthermore, IOE exhibited the lowest R_{TSS} (0.024) and R_{AUROC} (0.023), suggesting higher robustness compared with the FR and CF models (R_{TSS} of 0.04 and 0.05 and R_{AUROC} of 0.024 and 0.026). However, the variations are small, particularly in terms of AUROC.

4. Discussion

Geomorphic hazards are caused by imbalances in geomorphological systems; such imbalances result from external natural and human factors. Gully erosion is an example of a geomorphic hazard wherein a change in equilibrium occurs between topographical and hydrological parameters. Although the process is complex, the causes of gully erosion can be inferred using deterministic and statistical spatial models. Discovering cause-and-effect relationships is the key to identifying appropriate prevention and management techniques for gully development.

In this study, a probabilistic model (FR) and two statistical models (IOE and CF) were tested for GESM. Each model exhibits several advantages and disadvantages and demonstrates varying performance under different physiographic conditions. Therefore, a comparative evaluation can help identify the best model for each region’s conditions amongst the three. Simplicity, effective result interpretation and easy determination of the relationships between independent and dependent variables are amongst the advantages of the FR and CF methods. However, both methods cannot analyse the relationships between variables and the relative significance of the contributing factors (Lee and Pradhan, 2007; Yilmaz, 2009; Pradhan, 2010). The use of an entropy model to develop susceptibility classifications for the gully erosion process is relatively new but has been gaining popularity in the fields of geoscience and geomorphology (Zare et al., 2013; Fanos and Pradhan, 2019). This model does not require assumptions about the appropriate distribution of explanatory variables, and thus, several properties can be used and tested (Pourghasemi et al., 2012; Haghizadeh et al., 2017). Moreover, this method examines the statistical relationships between independent and dependent variables and provides metrics for the significance of the variables (Yufeng and Fengxiant, 2009).

The analysis shows that low elevations and areas with a small slope are more susceptible to gully erosion. This result can be ascribed to the concentration and stagnation of surface runoff and the coexistence of evaporation deposits (e.g. gypsum and salt), which are erosion-sensitive formations. This finding has been highlighted by many other contributions in which morphologic and geologic properties are assigned as determinants of the highest gully erosion susceptibility locations (Frankl et al., 2013; Rahmati et al., 2016; Arabameri et al., 2018b, c).

Other results suggest that distance to streams and roads, drainage density and NDVI are significant factors that promote favourable conditions for gullying. Areas that are close to streams and roads and have sparse vegetation and high drainage density exhibit a high potential for gully formation. These results are consistent with the findings of Nyssen et al. (2002), Campo-Bescós et al. (2013) and Azareh et al. (2019). Furthermore, limestone, sandstone, marl, shale and red conglomerate geology units are also associated with gullying. Although these conclusions are reflected in the model, these features are generally believed to promote gully erosion and have been previously identified in the study area (Palazón et al., 2014; Gessesse et al., 2015; Rafaello and Reis. 2016; Arabameri et al., 2018b, and Azareh et al., 2019).

Predictor importance assessment using the IOE model suggests that the simple combination of elevation, lithology and slope degree can explain the location of most of the gullies in the area. This statement may seem like an oversimplification, but the results are in line with the most recent findings in this research field (Arabameri et al., 2018c; Hosseinalizadeh et al., 2019; Arabameri and Pourghasemi, 2019). Hosseinalizadeh et al. (2019) used unmanned aerial vehicle data and four best-first decision classifier ensembles for the spatial modelling of gully head cuts in Golestan Province in Iran. They reported that land use, slope degree and slope length are the major gully drivers. Arabameri et al. (2018c) tested three data-driven models and an AHP-based technique for GESM in the Toroud Watershed in Semnan Province, Iran. They found that LULC, lithology and elevation factors control gully occurrence. Arabameri and Pourghasemi (2019) used quadratic discriminant analysis (QDA) and LDA models for gully erosion modelling in Shahroud Basin, Semnan Province, Iran. On the basis of the QDA results, LULC, drainage density and elevation models are the most important predictors of gully occurrence.

Prediction accuracy and robustness can be evaluated in the present study by using AUROC and TSS. The analyses indicated that the IOE model outperformed the two other models in terms of raw performance and robustness across bootstrapped replicates. This result is in line with the findings of Pourghasemi et al. (2012, 2013), Devkota et al. (2013), Wang et al. (2015), Chen et al. (2018) and Mohammady et al. (2012). Wang et al. (2015) used CF and IOE models for landslide susceptibility assessment in Qianyang County, Baoji City, China. The IOE model demonstrated higher predictive accuracy than the CF model. Chen et al. (2018) compared SVM with different kernel functions and IOE for landslide susceptibility mapping in Shangzhou District, China using 14 conditioning factors. They discovered that the IOE model exhibits the most satisfactory performance. The findings of the present study are consistent with the results reported in the literature.

5. Conclusions

The identification of effective factors in the initiation and development of gully erosion and mapping the distribution of sensitivity are prerequisites for understanding gully erosion and selecting the most appropriate control and damage reduction measures. The primary objective of this research was to compare and evaluate the IOE, FR and CF models and to identify the most important gully formation conditioning factors using these models. IOE indicated that elevation, lithology and slope angle can substantially explain gully erosion susceptibility patterns. Validation using 30% of the field-developed gully erosion location datasets showed that the IOE model performed better than FR and CF in terms of performance and robustness. Therefore, the IOE model was used as the reference model. IOE showed that 19.75% and 9.44% of the study area is under high and very high susceptibility classes, respectively. After examining the locations where high and very high probabilities were predicted and considering the identified important conditioning factors, several standard actions can be proposed to mitigate gullying in the area. These actions include the following: (i) executing engineering and water management measures to control and direct runoff; (ii) preventing runoff concentrations using flood diversion structures and the construction of gabions upstream; (iii) implementing management plans, such as restricting sheep herd size based on scientifically determined carrying capacities, and following vegetation management to protect locations that are susceptible to gullying and (iv) managing streams to reduce slope and slow down runoff. The GESM presented in this study can serve as a useful decision-making tool for managers, decision makers, engineers, urban planners and land use developers. A similar methodology can be used in other regions with similar physiographic and topographical features.

Funding

This research is financially supported by the UTS under grant numbers 323930 and 321740.2232335 and 321740.2232357.

References

Aghdam, I.N., Varzandeh, M.H.M., Pradhan, B., 2016. Landslide susceptibility mapping using an ensemble statistical index (Wi) and adaptive neuro-fuzzy inference system (ANFIS) model at Alborz Mountains (Iran). Environ. Earth Sci. 75 (7), 553. https://doi.org/10.1007/s12665-015-5233-6.

Angileri, S.E., Conoscenti, C., Hochschild, V., Märker, M., Rotigliano, E., Agnesi, V., 2016. Water erosion susceptibility mapping by applying stochastic gradient Treeboost to the Imera Meridionale River Basin (Sicily, Italy). Geomorphology 262, 61–76.

Allen, P.M., Arnold, J.G., Auguste, L., White, J., Dunbar, J., 2018. Application of a simple headcut advance model for gullies. Earth Surf. Proc. Land. 43, 202–217. https://doi.org/10.1002/esp.4233

Ali, S.A., Pirasteh, S. 2004. Geological applications of Landsat Enhanced Thematic Mapper (ETM) data and Geographic Information System (GIS): mapping and structural interpretation in south-west Iran, Zagros Structural Belt. Int. J. Remote Sens. 25 (21), 4715-4727.

Arekhi, S., Niazi, Y., 2010. Assessment of GIS and RS applications to estimate soil erosion and sediment loading by using RUSLE model (Case Study: upstream basin of Ilam dam). J. Soil Water Conserv. 17 (2), 1-27.

Alavi, M., 1994. Tectonics of Zagros Orogenic Belt of Iran, New Data and Interpretation. Tectonophysics 229, 211-238.

Amiri, M., Pourghasemi, H.R., Ghanbarian, G.A., Afzali, S.F., 2019. Assessment of the importance of gully erosion effective factors using Boruta algorithm and its spatial modeling and mapping using three machine learning algorithms. Geoderma 340, 55-69. https://doi.org/10.1016/j.geoderma.2018.12.042

Alilou, H., Rahmati, O., Singh, V. P., Choubin, B., Pradhan, B., Keesstra, S., et al. 2019. Evaluation of watershed health using Fuzzy-ANP approach considering geo-environmental and topo-hydrological criteria. J. Environ. Manage. 232, 22-36.

Arabameri, A., Pradhan, B., Rezaei, K., Yamani, M., Pourghasemi, H.R., Lombardo, L., 2018a. Spatial modelling of gully erosion using evidential belief function, logistic regression and a new ensemble EBF–LR algorithm. Land Degrad. Dev. 29 (11), 4035-4049. https://doi.org/10.1002/ldr.3151

Arabameri, A., Pradhan, B., Pourghasemi, H.R., Rezaei, K., Kerle, N., 2018b. Spatial modelling of gully erosion using GIS and R programing: a comparison among three data mining algorithms. Appl. Sci. 8 (8), 1369. https://doi.org/10.3390/app8081369

Arabameri, A., Rezaei, K., Pradhan, B., Pourghasemi, H.R., Lee, S., Yamani, M., 2018c. GIS-based gully erosion susceptibility mapping: a comparison among three data driven models and AHP knowledge-based technique. Environ. Earth Sci. 77, 628.

Arabameri, A., Pradhan, B., Pourghasemi, H.R., Rezaei, K., 2018d. Identification of erosion-prone areas using different multi-criteria decision-making techniques and GIS. Geomat. Nat. Haz. Risk 9, 1129-1155. https://doi.org/10.1080/19475705.2018.1513084

Arabameri, A., Pourghasemi, H.R., 2019. Spatial modeling of gully erosion using linear and quadratic discriminant analyses in GIS and R. Edit; Pourghasemi, H.R., Gokceoglu, C. Spatial modeling in GIS and R for Earth and Environmental Sciences. First edition. Elsevier publication. 796 p. https://doi.org/10.1016/B978-0-12-815226-3.00013-2

Arabameri, A., Pradhan, B., Rezaei, K., 2019a. Gully erosion zonation mapping using integrated geographically weighted regression with certainty factor and random forest models in GIS. J. Environ. Manage. 232, 928-942. https://doi.org/10.1016/j.jenvman.2018.11.110

Arabameri, A., Pradhan, B., Rezaei, K., 2019b. Spatial prediction of gully erosion using ALOS PALSAR data and ensemble bivariate and data mining models. Geosci. J. 23 (4), 669-686. https://doi.org/10.1007/s12303-018-0067-3

Arabameri, A., Pradhan, B., Rezaei, K., Conoscenti, C., 2019c. Gully erosion susceptibility mapping using GIS-based multi-criteria decision analysis techniques. Catena 180, 282–297.

Arabameri, A., Cerda, A., Tiefenbacher, J.P., 2019d. Spatial pattern analysis and prediction of gully erosion using novel hybrid model of entropy-weight of evidence. Water 11, 1129.

Arekhi, S., Niazi, Y., 2010. Assessment of GIS and RS applications to estimate soil erosion and sediment loading by using RUSLE model (Case Study: upstream basin of Ilam dam). J. Soil Water Conserv. 17(2), 1-27.

Antoneli, V., Rebinski, E. A., Bednarz, J. A., Rodrigo-Comino, J., Keesstra, S. D., Cerdà, A., Fernandez, M.P., 2018. Soil erosion induced by the introduction of new pasture species in a faxinal farm of Southern Brazil. Geosciences 8 (5), 166.

Azareh, A., Rahmati, O., Rafiei-Sardooi, E., Sankey, J.B., Lee, S., Shahabi, H., BinAhmad, B., 2019. Modelling gully-erosion susceptibility in a semi-arid region, Iran: Investigation of applicability of certainty factor and maximum entropy models. Sci. Total Environ. 655, 684-696. https://doi.org/10.1016/j.scitotenv.2018.11.235

Boreggio, M., Bernard, M., Gregoretti, C., 2018. Evaluating the influence of gridding techniques for Digital Elevation Models generation on the debris flow routing modeling: a case study from Rovina di Cancia basin (North-eastern Italian Alps). Front. Earth Sci. 6, 89.

Bout, B., Lombardo, L., van Westen, C.J., Jetten, V.G., 2018. Integration of two-phase solid fluid equations in a catchment model for flashfloods, debris flows and shallow slope failures. Environ. Model. Softw. 105, 1-16. https://doi.org/10.1016/j.envsoft.2018.03.017

Cama, M., Lombardo, L., Conoscenti, C., Rotigliano, E., 2017. Improving transferability strategies for debris flow susceptibility assessment: application to the Saponara and Itala catchments (Messina, Italy). Geomorphology 288, 52–65. https://doi.org/10.1016/j.geomorph.2017.03.025

Campo-Bescós, M., Flores-Cervantes, J., Bras, R., Casalí, J., Giráldez, J., 2013. Evaluation of a gully headcut retreat model using multitemporal aerial photographs and digital elevation models. J. Geophys. Res-Earth. 118, 2159-2173. https://doi.org/10.1002/jgrf.20147

Camilo, D.C., Lombardo, L., Mai, P.M., Dou, J., Huser, R., 2017. Handling high predictor dimensionality in slope-unit-based landslide susceptibility models through LASSO-penalized Generalized Linear Model. Environ. Model. Softw. 97, 145-156. https://doi.org/10.1016/j.envsoft.2017.08.003

Chen, W., Pourghasemi, H.R., Naghibi, S.A., 2018. A comparative study of landslide susceptibility maps produced using support vector machine with different kernel functions and entropy data mining models in China. B. Eng. Geol. Environ. 77(2), 647-664. https://doi.org/10.1007/s10064-017-1010-y

Conforti, M., Aucelli, P.P., Robustelli, G., Scarciglia, F., 2011. Geomorphology and GIS analysis for mapping gully erosion susceptibility in the Turbolo stream catchment (Northern Calabria, Italy). Nat. Hazards 56 (3), 881–898. https://doi.org/10.1007/s11069-010-9598-2

Conoscenti C, Angileri S, Cappadonia C, Rotigliano E, Agnesi V., Ma¨rker M., 2014. Gully erosion susceptibility assessment by means of GIS-based logistic regression: a case of Sicily (Italy). Geomorphology 204 (1), 399–411. https://doi.org/10.1016/j.geomorph.2013.08.021

Claps, P., Fiorentino, M., Oliveto, G., 1994. Informational entropy of fractal river networks. J. Hydrol. 187(1-2), 145-156 .

Dabral, P.P., Baithuri, N., Pandey, A., 2008. Soil erosion assessment in a hilly catchment of north eastern India using USLE, GIS and remote sensing. Water Resour. Manag. 22 (12), 1783-98. https://doi.org/10.1007/s11269-008-9253-9

Dehnavi, A., Aghdam, I.N., Pradhan, B., Varzandeh, M.H.M., 2015. A new hybrid model using step-wise weight assessment ratio analysis (SWARA) technique and adaptive neuro-fuzzy inference system (ANFIS) for regional landslide hazard assessment in Iran. Catena 135, 122–148. https://doi.org/10.1016/j.catena.2015.07.020.

Devkota, K.C., Regmi, A.D., Pourghasemi, H.R., Yoshida, K., Pradhan, B., Ryu, I.C., 2013. Landslide susceptibility mapping using certainty factor, index of entropy and logistic regression models in GIS and their comparison at Mugling–Narayanghat road section in Nepal Himalaya. Nat. Hazards 65 (1), 135–165. https://doi.org/10.1007/s11069-012-0347-6

Dube, F., Nhapi, I., Murwira, A., Gumindoga, W., Goldin, J., Mashauri, D.A., 2014. Potential of weight of evidence modelling for gully erosion hazard assessment in Mbire District—Zimbabwe. Phys. Chem. Earth. 67, 145–152. https://doi.org/10.1016/j.pce.2014.02.002

Evans, I. S., An integrated system of terrain analysis and slope mapping. Final Report on Grant DA-ERO-591-73-G0040, University of Durham, Durham, UK.

Fanos, A.M., Pradhan, B., 2019. Spatial ensemble model for rockfall source identification from high resolution LiDAR data and GIS. IEEE Access. 7, 74570–74585. https://doi.org/10.1109/ACCESS.2019.2919977.

Fernandes, J., Bateira, C., Soares, L., Faria, A., Oliveira, A., Hermenegildo, C., Moura, R., Gonçalves, J., 2017. SIMWE model application on susceptibility analysis to bank gully erosion in Alto Douro Wine Region agricultural terraces. Catena. 153, 39-49. https://doi.org/10.1016/j.catena.2017.01.034

Frankl, A., Zwertvaegher, A., Poesen, J., Nyssen, J., 2013. Transferring Google Earth Observations to GIS-software: example from gully erosion study. Int. J. Digit. Earth 6, 196-201. https://doi.org/10.1080/17538947.2012.744777

Fukuda, S., De Baets, B., Waegeman, W., Verwaeren, J., Mouton, A.M., 2013. Habitat prediction and knowledge extraction for spawning European grayling (Thymallus thymallus L.) using a broad range of species distribution models. Environ. Model. Softw. 47, 1–6. https://doi.org/10.1016/j.envsoft.2013.04.005

Galton, F., 1889. Narrative of an explorer in tropical South Africa: Being an account of a visit to Damaraland in 1851, vol 2. Ward, Lock and Company, pp. 320.

Gómez-Gutiérrez, A., Conoscenti, C., Angileri, S.E., Rotigliano, E., Schnabel, S., 2015. Using topographical attributes to evaluate gully erosion proneness (susceptibility) in two mediterranean basins: advantages and limitations. Nat. Hazards 79(1), 291–314. https://doi.org/10.1007/s11069-015-1703-0

Fressard, M., Thiery, Y., Maquaire, O., 2014. Which data for quantitative landslide susceptibility mapping at operational scale? Case study of the Pays d'Auge plateau hillslopes (Normandy, France). Nat. Hazard Earth Sys. 14 (3), 569–588

Geology Survey of Iran (GSI). 1997. http://www.gsi.ir/Main/Lang_en/ index .html

Gessesse, B., Bewket, W., Bräuning, A., 2015. Model-based characterization and monitoring of runoff and soil erosion in response to land use/land cover changes in the Modjo watershed, Ethiopia. Land Degrad. Dev. 26, 711-724, 10.1002/ldr.2276, 2015.

Gesch, D., Oimoen, M., Zhang, Z., Meyer, D., Danielson, J., 2012. Validation of the ASTER global digital elevation model version 2 over the conterminous United States. Int. Arch. Photogramm. Remote Sens. Spat. Inf. Sci. *B4*, 281–286.

Ghorbaninejad, S., Falah, F., Daneshfar, M., Haghizadeh, A., Rahmati, O. 2017.

Haghizadeh, A., Siahkamari, S., Haghiabi, A.H., Rahamti, O., 2017. Forecasting flood-prone areas using Shannon's entropy model. J. Earth Sys. Sci. 126, 39. https://doi.org/10.1007/s12040-017-0819-x

Hong, H., Naghibi, S.A., Dashtpagerdi, M.M., Pourghasemi, H.R., Chen, W., 2017. A comparative assessment between linear and quadratic discriminant analyses (LDAQDA) with frequency ratio and weights-of-evidence models for forest fire susceptibility mapping in China. Arab. J. Geosci. 10 (7), 167.

Hengl, T., 2006. Finding the right pixel size. Comput. Geosci. 32 (9), 1283- 1298. https://doi.org/10.1016/j.cageo.2005.11.008

Hosseinalizadeh, M., Kariminejad, N., Rahmati, O., Keesstra, S., Alinejad, M., Behbahani, A. M., 2019. How can statistical and artificial intelligence approaches predict piping erosion susceptibility?. Sci. Total Environ. 646, 1554-1566. https://doi.org/10.1016/j.scitotenv.2018.07.396

Heckerman, D., 1986. Probabilistic interpretation on MYCINs Certainty factors, In: Kanal, L. N., Lemmer, J. F. (Eds), uncertainty in Artificial Intelligence, Elsevier, New. York, pp. 298-311.

I.R. of Iran Meteorological Organization (IRIMO). 2012. Available online: http://www.mazan daranmet.ir.

Iqbaluddin, Ali, S. A., 1986, Photogeophysical approach to stress analysis in cratonic basin an example from Vindhyan basin, Rajasthan, India. Proceeding of the Seventh Asian Conference on Remote Sensing, Seoul, Korea, E-6-1–E-6-13.

Jones, K. H., 1998. A comparison of algorithms used to compute hill slope as a property of the DEM. Comput. Geosci. 24(4), 315–323.

Kornejady, A., Heidari, K., Nakhavali, M., 2015. Assessment of landslide susceptibility, semi-quantitative risk and management in the Ilam dam basin, Ilam. Iran. Environmental Resources Research 3 (1), 85–109. https://doi.org/10.22069/IJERR.2015.2563

Kiss, R., 2004. Determination of drainage network in digital elevation model. utilities and limitations Journal of Hungarian Geomathematics (2), 16-29.

Kornejady, A., Ownegh, M., Bahremand, A., 2017. Landslide susceptibility assessment using maximum entropy model with two different data sampling methods. Catena 152, 144–162. https://doi.org/10.1016/j.catena.2017.01.010

Lan, H. X., Zhou, C.H., Wang. L.J., Zhang, H. Y., Li, R. H., 2004. Landslide Hazard Spatial Analysis and Prediction Using GIS in the Xiaojing Watershed, Yunnan, China. Eng. Geol. 76, 109-128. 10.1007/s10064-006-0064-z

Lee, S., Pradhan, B., 2007. Landslide hazard mapping at Selangor, Malaysia using frequency ratio and logistic regression model. Landslides. 4, 33–41. https://doi.org/10.1007/s10346-006-0047-y

Lombardo, L., Mai, P.M., 2018. Presenting logistic regression-based landslide susceptibility results. Eng. Geol 244, 14-24. https://doi.org/10.1016/j.enggeo.2018.07.019

Lombardo, L., Opitz ,T., Huser, R., 2018a. Point process-based modeling of multiple debris flow landslides using INLA: an application to the 2009 Messina disaster. Stoch. Env. Res. Risk A. 2 (7), 2179-2198. https://doi.org/10.1007/s00477-018-1518-0

Lombardo, L., Saia, S., Schillaci, C., Mai, P.M., Huser, R., 2018b. Modeling soil organic carbon with Quantile Regression: Dissecting predictors' effects on carbon stocks. Geoderma 318, 148-159. https://doi.org/10.1016/j.geoderma.2017.12.011

Lucà, F., Conforti, M., Robustelli, G., 2011. Comparison of GIS-based gullying susceptibility mapping using bivariate and multivariate statistics: Northern Calabria, South Italy. Geomorphology 134, 297–308.

Lin, Z., Oguchi, T., 2004. Drainage density, slope angle, and relative basin position in Japanese bare lands from high-resolution DEMs. Geomorphology 63, 159–173.

Lin, W.T., Chou, W.C., Lin, C.Y., Huang, P.H., Tsai, J.S., 2006. Automated suitable drainage network extraction from digital elevation models in Taiwan's upstream watersheds. Hydrol. Process. 20, 289–306.

Mohammady, M., Pourghasemi, H.R., Pradhan, B., 2012. Landslide susceptibility mapping at Golestan Province, Iran: A comparison between frequency ratio, Dempster–Shafer, and weights-of-evidence models. J. Asian Earth Sci. 61 (15), 221-236. https://doi.org/10.1016/j.jseaes.2012.10.005

Mojaddadi, H., Pradhan, B., Nampak, H., Ahmad, N., Ghazali, A.H., 2017. Ensemble machine-learning-based geospatial approach for flood risk assessment using multi-sensor remote-sensing data and GIS, Geomat. Nat. Haz. Risk, 8 (2), 1080-1102, DOI: 10.1080/19475705.2017.1294113

Moore, I.D., Grayson, R.B., Ladson, A.R., 1991. Digital terrain modelling: a review of hydrological, geomorphological, and biological applications. Hydrol. Process. 5(1), 3–30.

Moore, I.D., Burch, G.J., 1986. Physical basis of the length-slopejuctor in the Universal soil loss equation. Soil Sci. Soc. Am. J. 50, 1294–1298.

Meliho, M., Khattabi, A., Mhammdi, N., 2018. A GIS-based approach for gully erosion susceptibility modelling using bivariate statistics methods in the Ourika watershed, Morocco. Environ. Earth Sci. 77, 655. https://doi.org/10.1007/s12665-018-7844-1

Naderi, F., Karimi, H., Naseri, B., 2015. Soil erosion potential zoning in Aseman Abad watershed by water erosion in Europe. Environ. Sci. Policy 54, 438-47. https://doi.org/10.22059/IJE.2018.239777.706

Nyssen, J., Poesen, J., Moeyersons, J., Luyten, E., Veyret-Picot, M., Deckers, J., et al. 2002. Impact of road building on gully erosion risk: a case study from the northern Ethiopian highlands. Earth Surf. Proc. Landf. 27, 1267-1283. https://doi.org/10.1002/esp.404

O'Brien, R.M., 2007. A caution regarding rules of thumb for variance inflation factors. Qual. Quant. 41 (5), 673–690. https://doi.org/10.1007/s11135-006-9018-6

Oh, H-J., Kim, Y-S., Choi, J-K., Park, E., Lee, S., 2011. GIS mapping of regional probabilistic groundwater potential in the area of Pohang City, Korea. J. Hydrol. 399 (3), 158-72. https://doi.org/10.1016/j.jhydrol.2010.12.027

O'Callaghan, J.F., Mark, D.M., 1984. The extraction of drainage networks from digital elevation data. Computer Vision, Graphics and Image Processing 28, 328-344. http://dx.doi.org/10.1016/S0734-189X(84)80011-0

Palazón, L., Gaspar, L., Latorre, B., Blake, W., Navas, A., 2014. Evaluating the importance of surface soil contributions to reservoir sediment in alpine environments: a combined modelling and fingerprinting approach in the Posets-Maladeta Natural Park. Solid Earth 5, 963, doi:10.5194/se-5-963-2014, 2014.

Pourghasemi, H. R., Mohammady, M., Pradhan, B., 2012. Landslide susceptibility mapping using index of entropy and conditional probability models in GIS: Safarood Basin, Iran. Catena 97, 71–84. https://doi.org/10.1016/j.catena.2012.05.005

Pourghasemi, H.R., Pradhan, B., Gokceoglu, C., Mohammadi, M., Moradi, H.R. 2013. Application of weights-of-evidence and certainty factor models and their comparison in landslide susceptibility mapping at Haraz watershed, Iran. Arab J. Geosci. 6 (7), 2351-2365. https://doi.org/10.1007/s12517-012-0532-7

Pradhan, B., 2010. Landslide susceptibility mapping of a catchment area using frequency ratio, fuzzy logic and multivariate logistic regression approaches. J. Indian Soc. Remote. 38, 301-320. https://doi.org/10.1007/s12524-010-0020-z

Pradhan, B., Lee, S., 2010. Regional landslide susceptibility analysis using backpropagation neural network model at Cameron Highland, Malaysia. Landslides 7 (1), 13–30. https://doi.org/10.1007/s10346-009-0183-2.

Planchon, O., Darboux, F., 2002. A fast, simple and versatile algorithm to fill the depressions of digital elevation models. Catena 46, 159-176.

Rafaello, B., Reis, E., 2016. Controlling factors of the size and location of large gully systems: A regression based exploration using reconstructed pre-erosion topography. Catena 147, 621-631. https://doi.org/10.1016/j.catena.2016.08.014

Ramsay, J. G., and Hubber, M., 1987, The Techniques of Modern Structural Geology, 2, Folds and Fractures (London: Academic Press). 307 P.

Ramasamy, S. N., 1985, Kinematic model for the evolution of Ramgarh Dome, Vindhyan basin Rajasthan. A study aided by remote sensing. PhD thesis submitted to Andhra University, India.

Rangzan, K., 1993, Structure and tectonics of the Zagros Belt, Iran. Unpublished PhD thesis, Aligarh Muslim University, Aligarh, India

Rahmati, O., Haghizadeh, A., Pourghasemi H.R., Noormohamadi, F., 2016. Gully erosion susceptibility mapping: the role of GIS based bivariate statistical models and their comparison. Nat. Hazards 82, 1231–1258. https://doi.org/10.1007/s11069-016-2239-7

Rahmati, O., Naghibi, S.A., Shahabi, H., Tien Bui, D., Pradhan, B., Azareh, A., et al. 2019. Groundwater spring potential modelling: Comprising the capability and robustness of three different modeling approaches. J. Hydrol. 565, 248-261. https://doi.org/10.1016/j.jhydrol.2018.08.027

Razavizadeh, S., Solaiman, K., Massironi, M., Kavian, A., 2017. Mapping landslide susceptibility with frequency ratio, statistical index, and weights of evidence models: a case study in northern Iran. Environ. Earth Sci. 76, 499. https://doi.org/10.1007/s12665-017-6839-7

Stocklin, J., 1968. Structural History and Tectonics of Iran A Review. Am. Assoc. Petr. Geol. B. 52, 1229-1258.

Shannon,C. E., 1948. A mathematical theory of Communication. Bull. Sys. Technol. J. 27, 379-423. https://doi.org/10.1002/j.1538-7305.1948.tb01338.x

Sharma, S., Kumar Mahajan, A., 2018. Comparative evaluation of GIS-based landslide susceptibility mapping using statistical and heuristic approach for Dharamshala region of Kangra Valley, India. Geoenvironmental Disasters 4, 4. https://doi.org/10.1186/s40677-018-0097-1

Tien Bui, D., Shirzadi, A., Shahabi, H., Chapi, K., Omidavr, E., Pham, B. T., Talebpour Asl, D., Khaledian, H., Pradhan, B., Panahi, M., 2019. A Novel Ensemble Artificial Intelligence Approach for Gully Erosion Mapping in a Semi-Arid Watershed (Iran). Sensors 19 (11), 2444.

Soil Survey Staff. 2014. Keys to soil taxonomy, 12th ed. USDA-Natural Resources Conservation Service, Washington DC.

Wang, G., Gertner, G., Fang, S., Anderson, A.B., 2003. Mapping multiple variables for predicting soil loss by geostatistical methods with TM images and a slope map. Photogramm. Eng. Rem. S. 69 (8), 889-98.

Wang, Q., Li, W., 2017. A GIS-based comparative evaluation of analytical hierarchy process and frequency ratio models for landslide susceptibility mapping. Phys. Geogr. 38 (4), 318-337.

Wang, Q., Li, W., Chen, W., Bai, H., 2015. GIS-based assessment of landslide susceptibility using certainty factor and index of entropy models for the Qianyang County of Baoji city, China. J. Earth Syst. Sci. 124 (7), 1399–1415. https://doi.org/10.1007/s12040-015-0624-3

Wu, C.Y., Mossa, J., Mao, L., Almulla, M., 2019. Comparison of different spatial interpolation methods for historical hydrographic data of the lowermost Mississipi River. Ann. GIS 25 (2), 133-151.

Yesilnacar, E.K., 2005. The application of computational intelligence to landslide susceptibility mapping in Turkey. Ph.D Thesis Department of Geomatics the University of Melbourne.

Yilmaz, I., 2009. Landslide susceptibility mapping using frequency ratio, logistic regression, artificial neural networks and their comparison (case study: Kat landslides). Comput. Geosci. 35, 1125-1138. https://doi.org/10.1016/j.cageo.2008.08.007

Youssef, A.M., Al-Kathery, M., Pradhan, B., 2015. Landslide susceptibility mapping at Al-Hasher area, Jizan (Saudi Arabia) using GIS-based frequency ratio and index of entropy models. Geosci. J. 19 (1), 113–134. https://doi.org/10.1007/s12303-014-0032-8.

Youssef, A.M., Pradhan, B., 2011. Flash flood risk estimation along the St. Katherine road, southern Sinai. Egypt us IS baseing Gd morphometry and satellite imagery. Environ. Earth Sci. 62(3),611‑623Yufeng, S., Fengxiant, J., 2009. Landslide stability analysis based on generalized information entropy. International Conference on Environmental Science and Information Application Technology. 83-85.

Zare, M., Pourghasemi, H.R., Vafakhah, M., Pradhan, B., 2013. Landslide susceptibility mapping

at Vaz Watershed (Iran) using an artificial neural network model: a comparison between multilayer perceptron (MLP) and radial basic function (RBF) algorithms. Arab. J. Geosci. 6 (8), 2873–2888. https://doi.org/10.1007/s12517-012-0610-x.

Zhou, C., Ge, L.E.D., Chang, H.C., 2005. A case study of using external DEM in InSAR DEM generation. Geo-Spat. Inf. Sci. *8*, 14–18

Zhou, Q., Liu, X., 2004. Analysis of errors of derived slope and aspect related to DEM data properties. Comput. Geosci. 30(4), 369–378.

Zhang, W., Wang, W., Chen, L., 2012. Constructing DEM based on InSAR and the relationship between InSAR DEM's precision and terrain factors. Energy Procedia 16, 184–189.

Zakerinejad, R., Maerker, M., 2014. Prediction of gully erosion susceptibilities using detailed terrain analysis and maximum entropy modeling: a case study in the Mazayejan Plain, Southwest Iran. Supplementi di Geografia Fisica e Dinamica Quaternaria. 37(1), 67–76. https://doi.org/10.4461/GFDQ.2014.37.7

Highlights

- Spatial gully erosion assessment was performed at the Ardib River Watershed
- Three predictive models were tested to assess gully-erosion-susceptibility mapping
- Models are combined with remote sensing (RS) and (GIS) to predict gully development
- Index of entropy (IOE) was found as the most accurate model
- Almost 1/3 of the watershed showed high or very high susceptibility to gully

Table 1. Lithology of study area

Group	Unit	Description	Age
	E1c	Pale-red, polygenic conglomerate and sandstone	Paleocene-Eocene
A	Ed.avs	Dacitic to Andesitic volcanosediment	Eocene
	Egr	Granite	Eocene
	Jub	Sandstone, siltstone, Pectinid limestone, marl, gypsum (Bidou Series)	Late Jurassic
B	Jugr	Upper Jurassic granite including Shir Kuh Granite and Shah Kuh Granite	Late Jurassic
	Jurb	Sandstone, siltstone, and fine grained conglomerate (Garedu red beds)	Late Jurassic
	K2lm	Pale - red marl, gypsiferous marl and limestone	Late Cretaceous
	K2l2	Thick - bedded to massive limestone (maastrichtian)	Late Cretaceous
	Kdzsh	Marl, shale, sandstone and limestone (Darreh - Zanjir Fm)	Cretaceous
	K2m,l	Marl, shale and detritic limestone	Late Cretaceous
C	Ktl	Thin to meddium bedded argillaceous limestone and thick bedded to massive, grey orbitolina bearing limestone (Taft Fm)	Early Cretaceous
	Kns	Red sandstone and conglomeratic sandstone	Early Cretaceous
	Kbsh	Dark grey slightly phyllitized shale with intercalations of sandstone and limestone (Biabanak Shale)	Cretaceous
	K1c	Red conglomerate and sandstone	Cretaceous
	K2d.asv	Dacitic to andesitic subvolcanic rocks	Late Cretaceous
D	Murm	Ligth - red to brown marl and gypsiferous marl with sandstone intercalations	Miocene
	mb	Marble	Triassic
	Pj	Massive to thick - bedded, dark - grey, partly reef type limestone and a thick yellow dolomite band in the upper part	Permian
	pCmt2	Low - grade, regional metamorphic rocks (Green Schist Facies)	Pre-Cambrian
	Plc	Polymictic conglomerate and sandstone	Pliocene
E	pCgn	Gneiss, granite gneiss and locally including migmatite	Pre-Cambrian
	P	Undifferentiated Permian rocks	Permian
	Pel	Medium to thick - bedded limestone	Paleocene-Eocene
	Pz	Undifferentiated lower Paleozoic rocks	Early Paleozoic
	pCdi	Precambrian diorite	Pre-Cambrian
	Qft2	Low level piedmont fan and valley terrace deposits	Quaternary
	Qsf	Salt flat	Quaternary
F	Qs,d	Unconsolidated wind-blown sand deposits including sand dunes	Quaternary
	Qft1	High level piedmont fan and valley terrace deposits	Quaternary
	Qsl	salt lake	Quaternary
G	TRJs	Dark grey shale and sandstone	Triassic-Jurassic

Table 2. Techniques used for the construction of various thematic data layers.

No	Factor	Data used & Scale	Sources of Data Types	Classes	Classification Method	References
1	Elevation (m)	ALOS DEM 12.5 m × 12.5	U.S Geological Survey	1. <802, 2. 802-954, 3. 954-1122, 4. 1122-1300, 5. 1300-1549, 6. >1549	Natural break	Arabameri et al., 2018e
2	Slope (˚)	ALOS DEM 12.5 m × 12.5	U.S Geological Survey	1. <5, 2. 5-10, 3. 10-15, 4. 15-20, 5. 20-30, 6. >30	Manual	Luca et al., 2011
3	Aspect	ALOS DEM 12.5 m × 12.5	U.S Geological Survey	1. F, 2. N, 3. NE, 4. E, 5. SE, 6. S, 7. SW, 8.W, 9. NW	Azimuth	Arabameri et al., 2019d
4	Plan curvature (m^{-1})	ALOS DEM 12.5 m × 12.5	U.S Geological Survey	1. Concave, 2. Flat, 3. Convex	Manual	Arabameri et al., 2019d
5	CI	ALOS DEM 12.5 m × 12.5	U.S Geological Survey	1. <-38.8, 2. -38.8 - -12.1, 3. -12.1 – 11.3, 4. 11.3 – 38, 5. >38	Natural break	Arabameri et al., 2018e
6	TWI	ALOS DEM 12.5 m × 12.5	U.S Geological Survey	1. <5.6, 2. 5.6-8.1, 3. 8.1-11.7, 4. >11.7	Natural break	Arabameri et al., 2019d
7	SPI	ALOS DEM 12.5 m × 12.5	U.S Geological Survey	1. <8, 2. 8-9.5, 3. 9.5-11.1, 4. 11.1-13.1, 5. 13.1 - 15.8, 6. >15.8	Natural break	Conforti et al., 2011
8	LS (m)	ALOS DEM 12.5 m × 12.5	U.S Geological Survey	1. <7, 2. 7 – 10, 3. 10 – 13.5, 4. 13.5 – 17.5, 5. 17.5 – 22.9, 6. >22.9	Natural break	Arabameri et al., 2018e
9	Lithology	Reference geological map 1: 50,000	Geological Survey of India	1. A, 2. B, 3. C, 4. D, 5. E, 6. F, 7. G	Lithology type	-
10	Soil	Reference district soil map 1: 100,000	Isfahan Agricultural and Natural Resources Research Centre	1. Dune Lands, 2. Playa, 3. Rocky Lands/Entisols, 4. Salt Flats, 5. Aridisols, 6. Entisols/Aridisols	Soil type	-
11	Distance to river (m)	ALOS DEM 12.5 m × 12.5	U.S Geological Survey	1. <100, 2. 100 – 200, 3. 200 – 300, 4. 300 – 400, 5. >400	Manual	Arabameri et al., 2018c
12	Drainage density (km/km2)	ALOS DEM 12.5 m × 12.5	U.S Geological Survey	1. <0.89, 2. 0.89 – 1.34, 3. 1.34 – 1.9, 4. >1.9	Natural break	Rahmati et al., 2016
13	Distance to fault (m)	Landsat-7 ETM+ image 30 m × 30	U.S Geological Survey	1. <500, 2. 500 – 1000, 3. 1000 – 1500, 4. 1500 – 2000, 5. > 2500	Manual	Tien Bui et al., 2019
14	LULC	Landsat 8 OLI/TIRS 30 m × 30	U.S Geological Survey	1. Agriculture (A), 2. Bareland (B), 3. Saltland-poor-pasture (C), 4. Sanddune (D), 5. Wetland (E), 6. Midrange (F), 7. Poor-pasture (G), 8. Saltlake (H), 9. Saltland (I), 10. Urban (G), 11. Wetland (k), 12. Woodland (L)	Land use type	-
15	NDVI	Landsat 8 OLI/TIRS 30 m × 30	U.S Geological Survey	1. <0.044, 2. 0.044 – 0.12, 3. >0.12	Natural break	Arabameri et al., 2018e
16	Distance to road (m)	Reference Topomap 1: 50,000	National Geographic Organization of Iran	1. <500, 2. 500 – 1000, 3. 1000 – 1500, 4. 1500 – 2000, 5. > 2500	Manual	Arabameri et al., 2019a

Table 3. Multi-collinearity among conditioning factors

Factors	Multicollinearity	
	TOL	**VIF**
Soil type	0.405	2.46
LU/LC	0.582	1.71
Slope aspect	0.339	2.95
Convergence index	0.724	1.38
Elevation	0.986	1.11
Distance to stream	0.826	1.21
Distance to fault	0.447	2.24
Distance to road	0.524	1.9
Drainage density	0.612	1.63
LS	0.490	2.1
SPI	0.211	4.23
TWI	0.25	4.1
Lithology	0.574	1.74
NDVI	0.838	1.19
Plan curvature	0.695	1.43
Slope	0.339	2.95
Rainfall	0.032	31.64
Soil texture	0.022	45.23
Catchment area	0.028	35.65

Table 4. Spatial relationship between gully erosion conditioning factors and gully locations using frequency ratio (FR), certainty factor (CF), and index of entropy (IOE).

Factors	Classes	Pixels in domain		gullies		CF	FR	FR and IOE models		
		Count	%	Count	%		FR	Ij	Mean Pij	Wj
Elevation (m)	<802	2074755	44.35	38	17.92	-0.60	0.40	1.74	0.93	1.61
	802-954	896820	19.17	119	56.13	1.93	2.93			
	954-1122	624848	13.36	28	13.21	-0.01	0.99			
	1122-1300	633063	13.53	17	8.02	-0.41	0.59			
	1300-1549	340011	7.27	10	4.72	-0.35	0.65			
	>1549	108301	2.32	0	0.00	-1.00	0.00			
Slope (°)	<5	3743855	80.03	168	79.25	-0.01	0.99	0.68	0.63	0.43
	5-10	387657	8.29	40	18.87	0.68	2.28			
	10-15	181868	3.89	4	1.89	-0.51	0.49			
	15-20	118930	2.54	0	0.00	-1.00	0.00			
	20-30	147808	3.16	0	0.00	-1.00	0.00			
	>30	97680	2.09	0	0.00	-1.00	0.00			
Aspect	F	185508	3.97	1	0.47	-0.88	0.12	0.07	0.93	0.07
	N	688408	14.72	23	10.85	-0.26	0.74			
	NE	761867	16.29	22	10.38	-0.36	0.64			
	E	734753	15.71	52	24.53	0.56	1.56			
	SE	540958	11.56	45	21.23	0.84	1.84			
	S	406712	8.69	9	4.25	-0.51	0.49			
	SW	352979	7.55	16	7.55	0.00	1.00			
	W	433236	9.26	22	10.38	0.12	1.12			
	NW	573377	12.26	22	10.38	-0.15	0.85			
Plan Curvature (100/m)	Concave	1480721	31.65	70	33.02	0.04	1.04	0.00	1.00	0.00
	Flat	1681964	35.96	74	34.91	-0.03	0.97			
	Convex	1515111	32.39	68	32.08	-0.01	0.99			
TWI	<5.6	1272339	27.20	60	28.30	0.04	1.04	0.02	1.07	0.02
	5.6-8.1	2219028	47.44	102	48.11	0.01	1.01			
	8.1-11.7	923908	19.75	33	15.57	-0.27	0.79			
	>11.7	262523	5.61	17	8.02	0.30	1.43			
SPI	<8	1389365	29.70	55	25.94	-0.14	0.87	0.03	1.16	0.03
	8-9.5	1522973	32.56	71	33.49	0.03	1.03			
	9.5-11.1	1099249	23.50	47	22.17	-0.06	0.94			
	11.1-13.1	469987	10.05	23	10.85	0.07	1.08			
	13.1 - 15.8	151017	3.23	14	6.60	0.51	2.05			
	>15.8	45206	0.97	2	0.94	-0.02	0.98			
Convergence	<-38.8	491199	10.51	12	5.66	-0.46	0.54	0.03	0.92	0.03
	-38.8 - -12.1	1077232	23.05	43	20.28	-0.12	0.88			
	-12.1 – 11.3	1540618	32.96	97	45.75	0.39	1.39			
	11.3 – 38	1053204	22.53	35	16.51	-0.27	0.73			
	>38	511753	10.95	25	11.79	0.08	1.08			
LS (m)	<7	1212314	25.92	46	21.70	-0.19	0.84	0.05	1.26	0.07
	7 – 10	1530683	32.72	68	32.08	-0.02	0.98			
	10 – 13.5	1038302	22.20	47	22.17	0.00	1.00			
	13.5 – 17.5	550711	11.77	29	13.68	0.14	1.16			
	17.5 – 22.9	260403	5.57	12	5.66	0.02	1.02			
	>22.9	85384	1.83	10	4.72	0.61	2.58			
Deainage density (km/km2)	<0.89	1000973	21.40	23	10.85	-0.49	0.51	0.29	0.72	0.21
	0.89 – 1.34	1917446	40.99	140	66.04	0.61	1.61			
	1.34 – 1.9	1409790	30.14	49	23.11	-0.23	0.77			
	>1.9	349589	7.47	0	0.00	-1.00	0.00			
Dis to stream (m)	<100	1127741	24.11	62	29.25	0.18	1.21	0.01	0.96	0.01
	100 – 200	886137	18.94	34	16.04	-0.18	0.85			
	200 – 300	773765	16.54	35	16.51	0.00	1.00			
	300 - 400	521331	11.14	16	7.55	-0.48	0.68			
	>400	1368823	29.26	65	30.66	0.05	1.05			
Dis to road (m)	<500	138959	2.97	24	11.32	0.74	3.81	0.10	3.76	0.36
	500 – 1000	132004	2.82	31	14.62	0.81	5.18			

	1000 – 1500	129203	2.76	34	16.04	0.83	5.81			
	1500 – 2000	128206	2.74	20	9.43	0.71	3.44			
	> 2500	4149426	88.70	103	48.58	-0.83	0.55			
Dis to fault (m)	<500	179354	3.83	15	7.08	0.85	1.85	0.15	1.01	0.16
	500 – 1000	174402	3.73	13	6.13	0.64	1.64			
	1000 – 1500	160714	3.44	3	1.42	-0.59	0.41			
	1500 – 2000	149649	3.20	1	0.47	-0.85	0.15			
	> 2500	4013679	85.80	180	84.91	-0.01	0.99			
NDVI	<0.044	2550134	54.52	68	32.08	-0.41	0.59	0.46	0.69	0.32
	0.044 – 0.12	2124332	45.42	144	67.92	0.50	1.50			
	>0.12	2756	0.06	0	0.00	-1.00	0.00			
LU/LC	Agriculture (A)	6123	0.13	0	0.00	-1.00	0.00	0.42	0.46	0.20
	Bareland (B)	437295	9.35	10	4.72	-0.50	0.50			
	Saltland-poor-pasture (C)	777200	16.61	31	14.62	-0.12	0.88			
	Sanddune (D)	460743	9.85	0	0.00	-1.00	0.00			
	Wetland (E)	50158	1.07	0	0.00	-1.00	0.00			
	Midrange (F)	625869	13.38	5	2.36	-0.82	0.18			
	Poor-pasture (G)	1709386	36.54	159	75.00	1.05	2.05			
	Saltlake (H)	216997	4.64	0	0.00	-1.00	0.00			
	Saltland (I)	71688	1.53	6	2.83	0.85	1.85			
	Urban (G)	640	0.01	0	0.00	-1.00	0.00			
	Wetland (k)	135854	2.90	0	0.00	-1.00	0.00			
	Woodland (L)	185844	3.97	1	0.47	-0.88	0.12			
Soil type	Dune Lands	472039	10.09	0	0.00	-1.00	0.00	0.28	0.64	0.18
	Playa	297806	6.37	8	3.77	-0.41	0.59			
	Rocky Lands/Entisols	1506557	32.21	94	44.34	0.35	1.35			
	Salt Flats	830784	17.76	19	8.96	-0.50	0.50			
	Aridisols	1492614	31.91	91	42.92	0.38	1.38			
	Entisols/Aridisols	77998	1.67	0	0.00	-1.00	0.00			
Lithology	A	40648	0.87	0	0.00	-1.00	0.00	0.75	0.58	0.44
	B	108225	2.31	0	0.00	-1.00	0.00			
	C	957383	20.47	153	72.17	1.00	3.53			
	D	166115	3.55	1	0.47	-0.87	0.13			
	E	419510	8.97	0	0.00	-1.00	0.00			
	F	2955028	63.17	58	27.36	-0.57	0.43			
	G	30889	0.66	0	0.00	-1.00	0.00			

Table 5. Percentage of susceptibility classes along with seed cell area index (SCAI)

	Value	Pixels in domain		Gullies		SCAI
		Count	%	Count	%	
FR	Very Low	1135939	24.29	5	1.68	14.43
	Low	2088424.	44.65	60	20.20	2.21
	Moderate	671346	14.35	15	5.05	2.84
	High	676182	14.46	67	22.56	0.64
	Very High	105232	2.25	150	50.51	0.04
CF	Very Low	1019405	21.80	2	0.67	32.37
	Low	1636833	35.00	47	15.82	2.21
	Moderate	1066969	22.81	23	7.74	2.95
	High	714980	15.29	53	17.85	0.86
	Very High	238936	5.11	172	57.91	0.09
IOE	Very Low	721185	15.42	1	0.34	45.80
	Low	1237659	26.46	16	5.39	4.91
	Moderate	1352819	28.92	41	13.80	2.10
	High	923752	19.75	40	13.47	1.47
	Very High	441708	9.44	199	67.00	0.14

Table 6. Values of ROC and TSS in six sample points and their average

Validation	Models	1	2	3	4	5	6	Mean
ROC	IOE	0.877	0.894	0.876	0.865	0.866	0.871	0.874
	FR	0.865	0.883	0.874	0.859	0.865	0.863	0.868
	CF	0.872	0.879	0.871	0.853	0.858	0.859	0.865
TSS	IOE	0.855	0.879	0.870	0.864	0.855	0.863	0.864
	FR	0.830	0.870	0.856	0.852	0.842	0.859	0.851
	CF	0.811	0.861	0.839	0.853	0.829	0.85	0.84

Figure

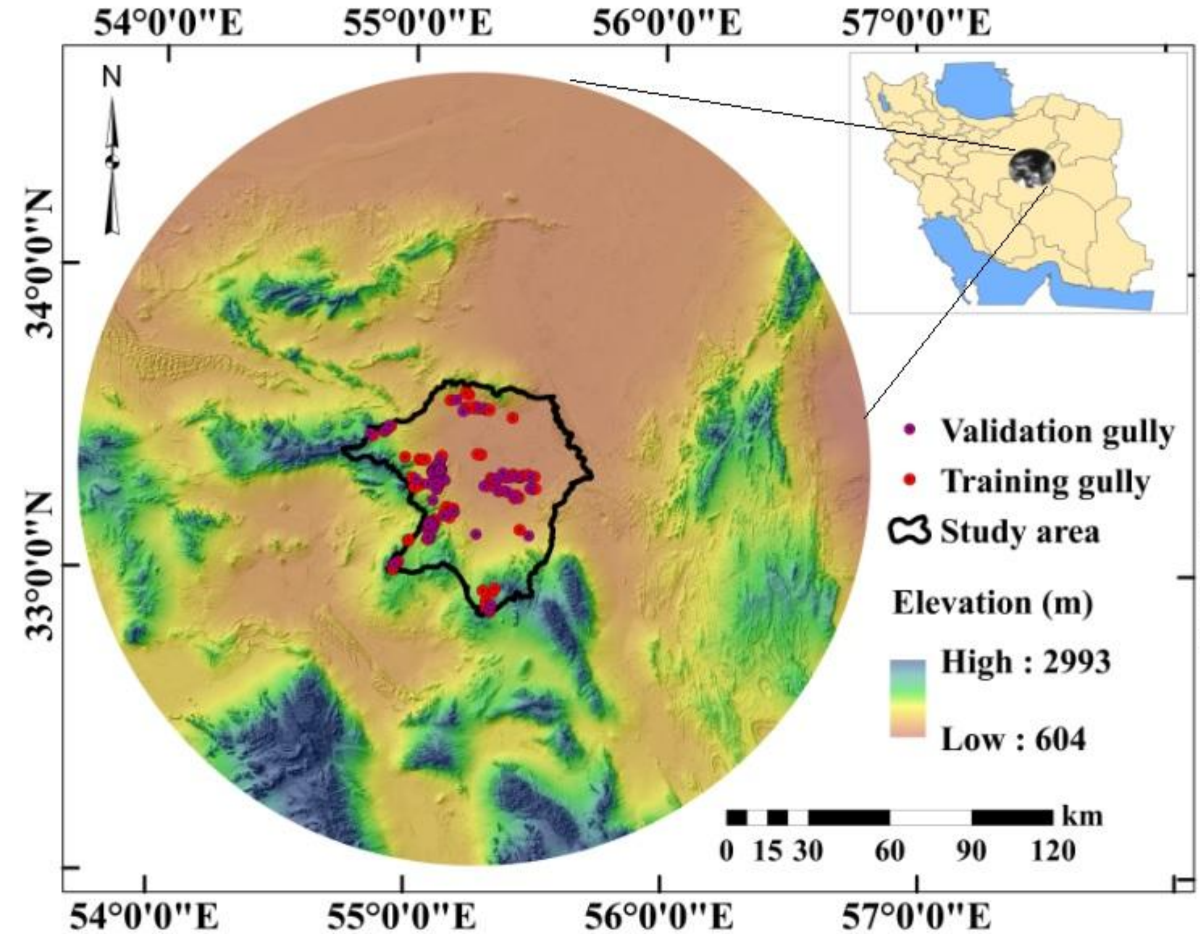

Fig 1. Location of study area in Iran

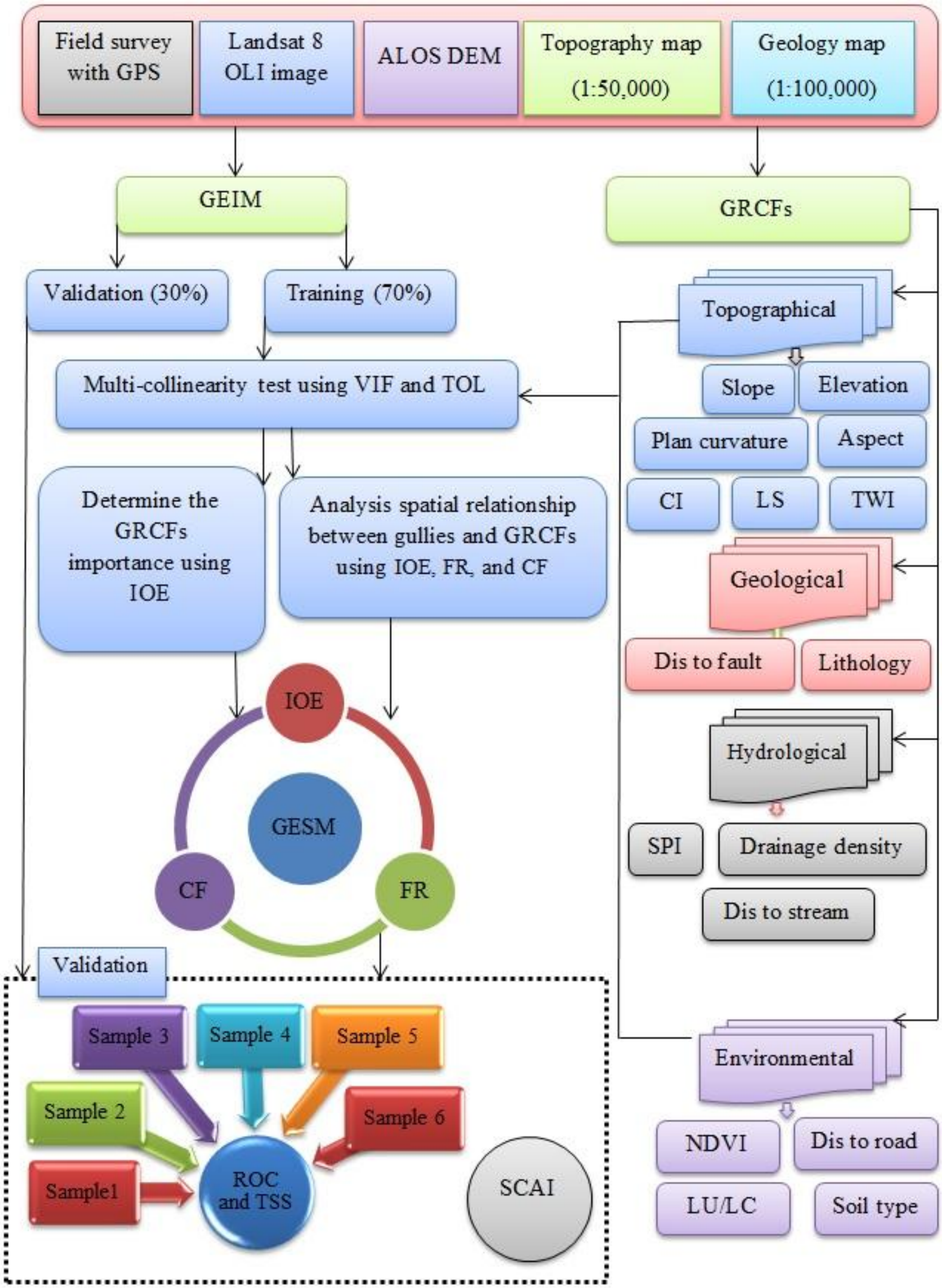

Fig 2. Flowchart of research

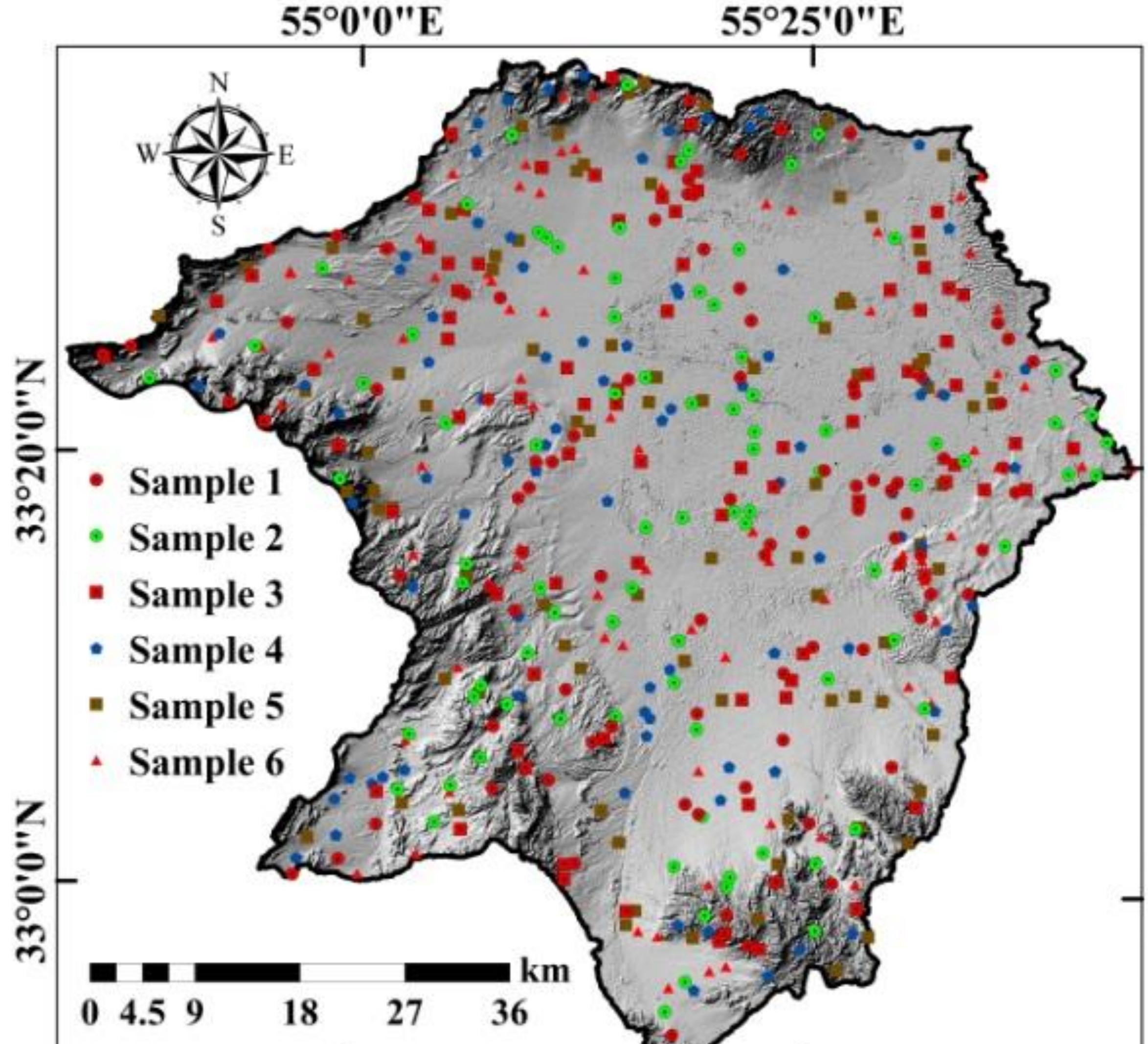

Fig 3. Six set of sample points for calculation of mean of ROC

Fig 4. Field photograph showing gullies in the study area (South of Ardib)

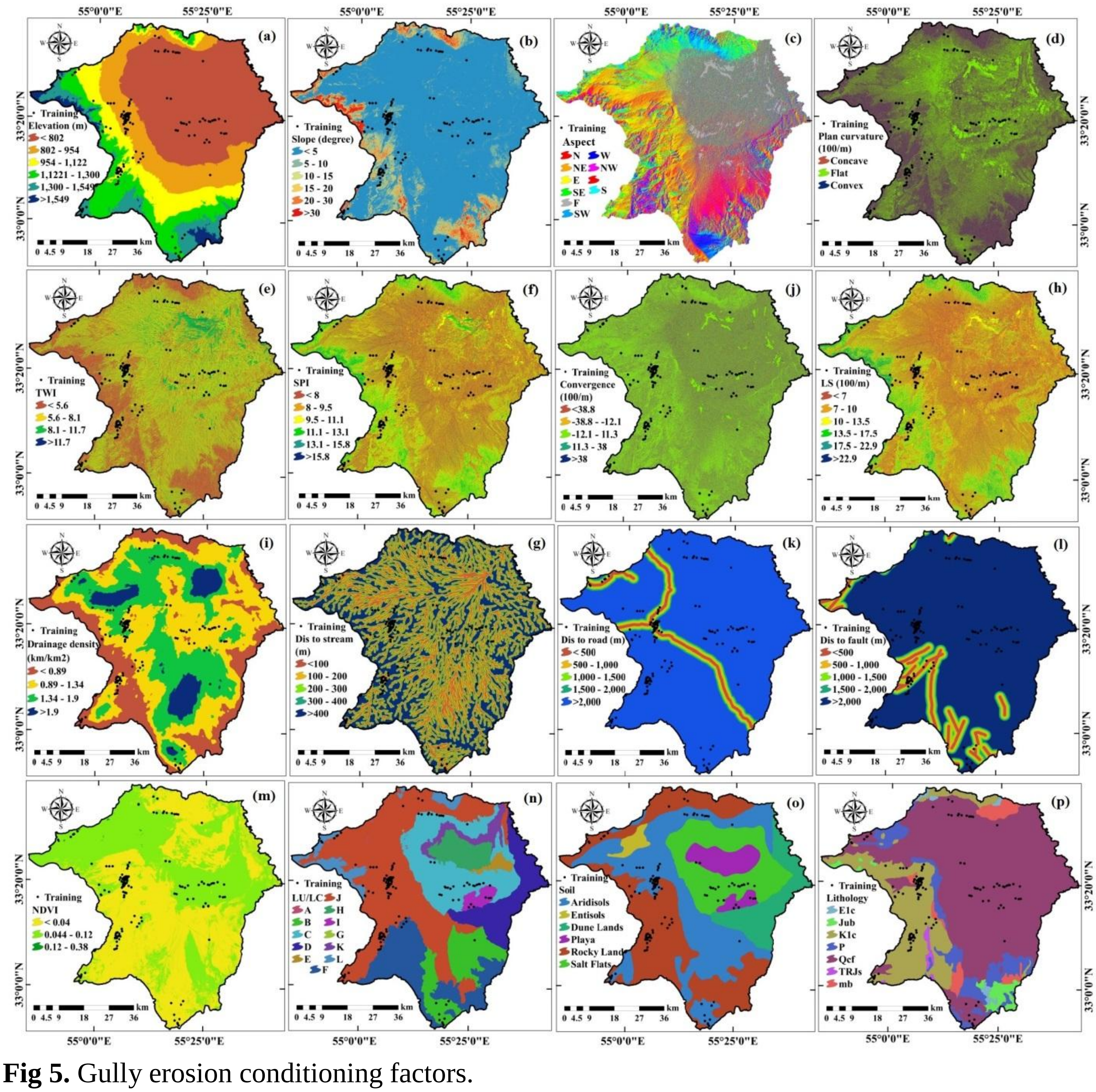

Fig 5. Gully erosion conditioning factors.

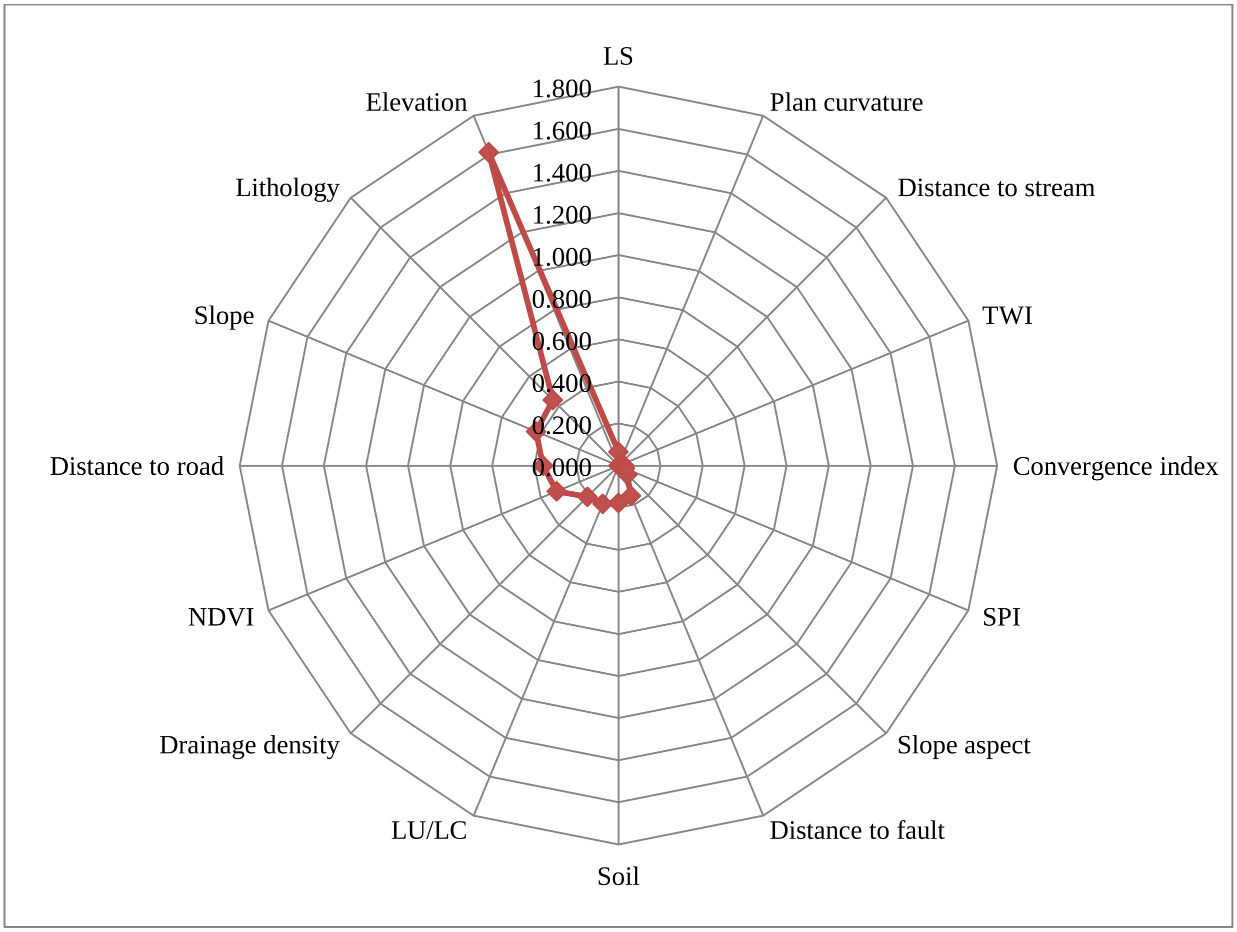

Fig 6. Relative importance of conditioning factors using index of entropy model

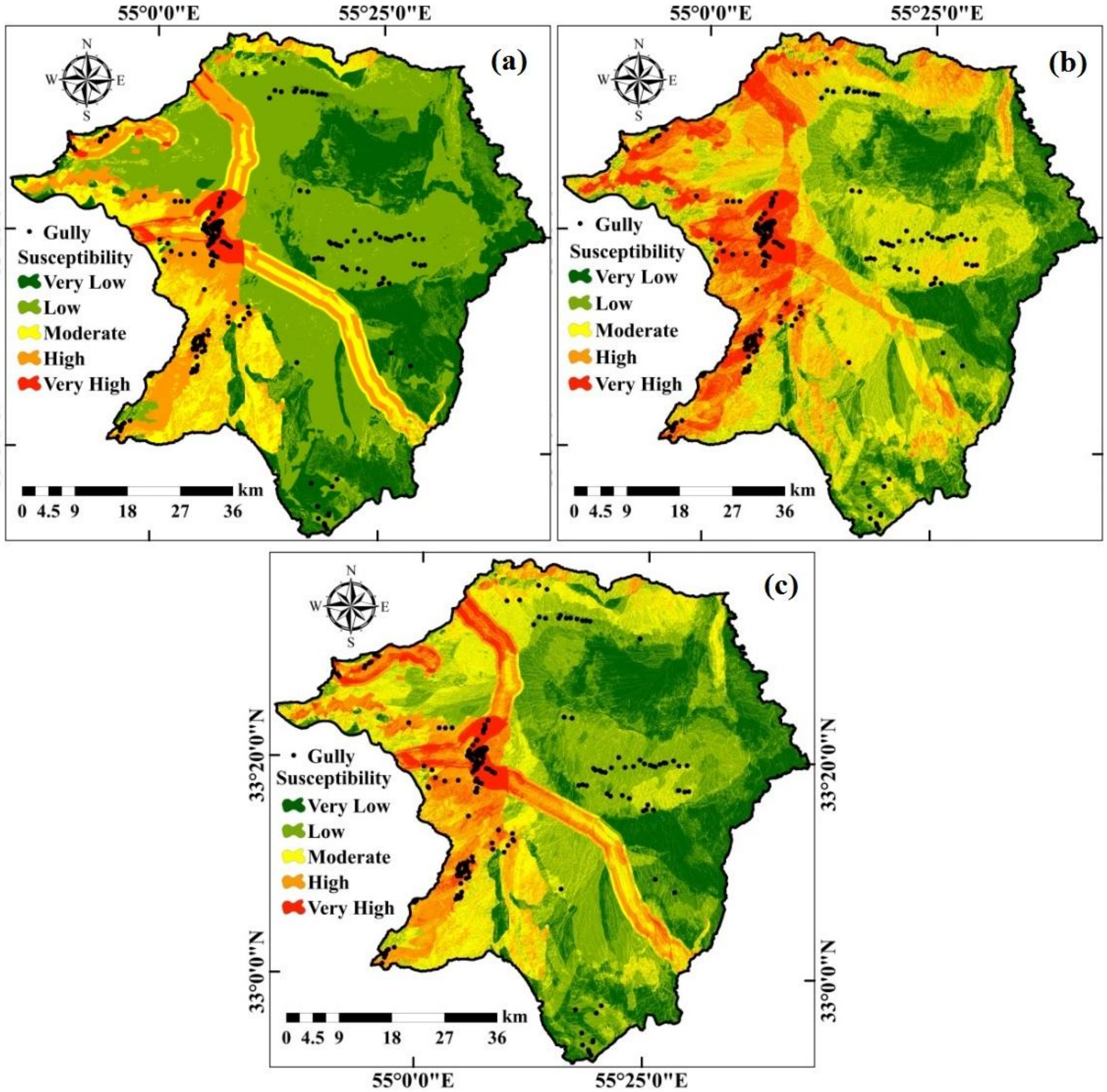

Fig 7. Gully erosion susceptibility map using different models. a) Frequency ration, b) index of entropy, c) certainty factor

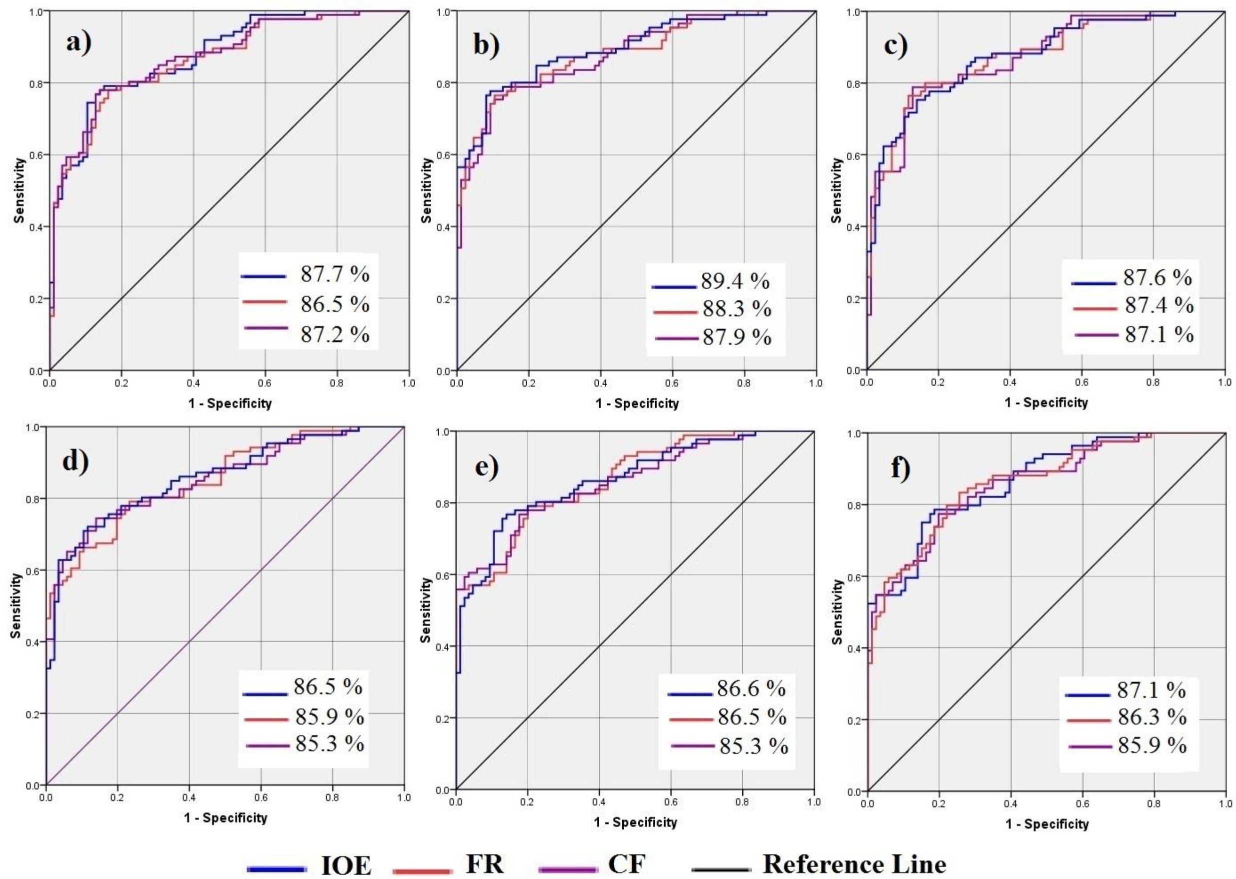

Fig 8. Roc curve for six different sample points. a) sample 1, b) sample 2, c) sample 3, d) sample 4, e) sample 5, f) sample 6.

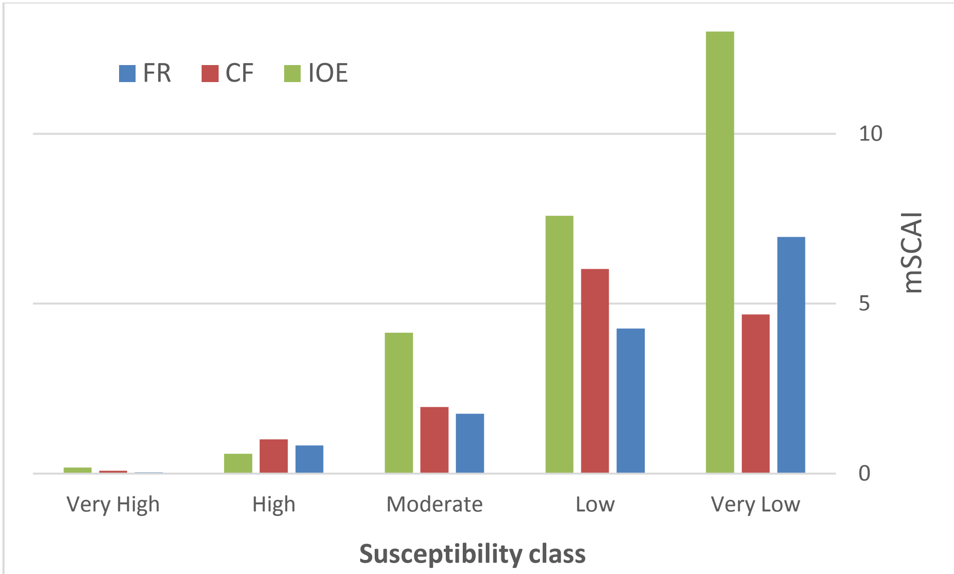

Fig 9. mSCAI values for susceptibility classes of the three developed maps.

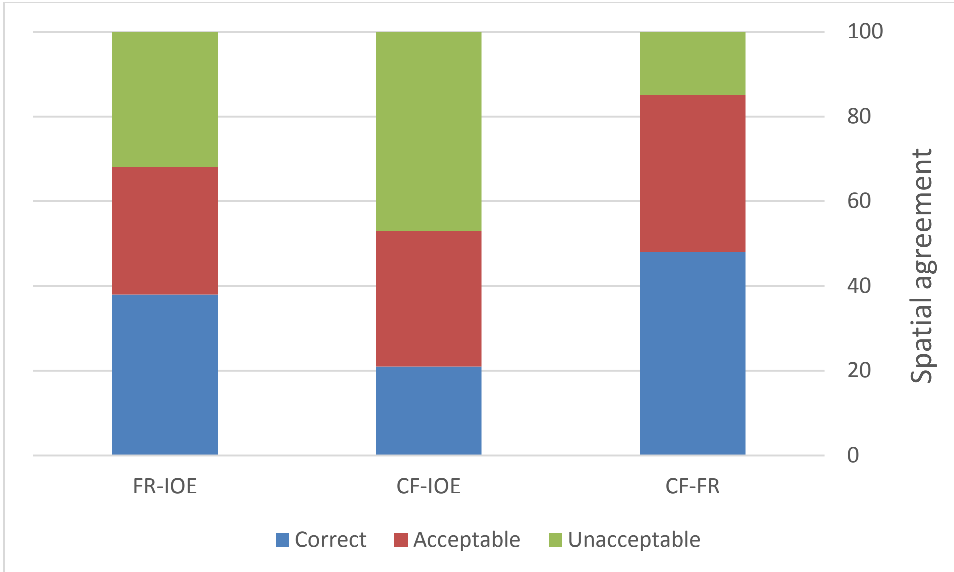

Fig 10. Degree of spatial agreement between the four susceptibility maps

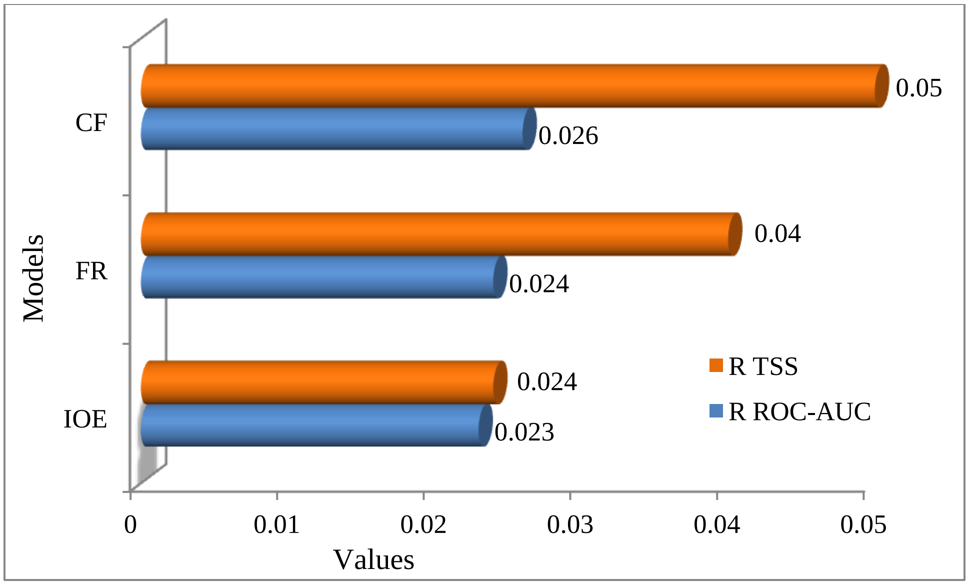

Fig 11. Robustness of the applied models in validation steps